40 Years of Full-Scale Infrastructure Testing at a National Geotechnical Experimentation Site: Sand Site.

Jean-Louis Briaud, *Distinguished Professor, Zachry Dpt. of Civil Engineering, Texas A&M University, College Station, Texas, 77834-3136, U.S.A.; email: briaud@tamu.edu*

ABSTRACT*: A site at the Texas A&M University RELLIS campus near College Station, Texas, was dedicated to full-scale infrastructure testing in 1978. It was designated as a National Geotechnical Experimentation Site by NSF and FHWA in 1992. The site is made of 15 m of medium dense silty sand, within which most experiments took place, underlain by a deep layer of clay shale. The water table is approximately 7.5 m deep. Over the last 40 years, many full-scale instrumented experiments on infrastructure elements have been conducted at that site. The main projects include a box culvert within an embankment, spread footings of various sizes, drilled shafts with intentional construction defects, an anchored top down retaining wall, a top down deep-soil-mixing retaining wall, post grouted drilled shafts, vibro-driven steel piles, a drilled shaft embedded in an MSE wall and pushing on it, a tractor trailer truck crashing against a barrier on top of an MSE wall, a single unit truck crashing against a row of in line piles, and erosion in-situ tests. This paper describes each one of those projects and also presents the results and lessons learned from these full-scale infrastructure tests and associated soil tests; references to related reports are provided for further details regarding each project.*

KEYWORDS: embankment, shallow foundations, deep foundations, retaining walls, culverts, in-situ testing, laboratory tests, full-scale testing, infrastructure elements, vehicle crash testing, sand.

SITE LOCATION: Geo-Database

INTRODUCTION

This paper follows the paper describing the work done at the Texas A&M University National Geotechnical Experimentation Site (NGES): Clay site (Briaud, 2021). Some of the common introductory material is not repeated. Since 1978, many projects have been conducted mostly by the author but also by colleagues from the U.S.A. and other countries. The main projects at the sand site are described in this paper and include a box culvert within an embankment, spread footings of various sizes, drilled shafts with intentional construction defects, an anchored top down retaining wall, a 10 m high – 50 m long top down deep-soil-mixing retaining wall, post grouted drilled shafts, vibro-driven steel piles, a drilled shaft embedded in an MSE wall and pushing on it, a tractor trailer truck crashing against a barrier on top of an MSE wall, a single unit truck crashing against a row of in line piles, and erosion in-situ tests. Within this paper, each one of those projects is described, and the results and lessons learned from these full-scale infrastructure tests and associated soil tests are reported.

THE SAND AND THE SITE GEOLOGY

The stratigraphy of the site is as follows (Fig. 1, Briaud, 1997). The first layer is a 4 m thick red and tan silty sand layer of the Pleistocene Age, deposited by fluvial and overbank flow. The second layer is a 4 m thick, clean sand layer of the Pleistocene Age, likely deposited by an extremely sand-laden small meandering stream. The third layer is also of the Pleistocene Age; it is 4.5 m thick and made of thin interbedded sand, clay, and clayey gravel layers. It was likely deposited by a small stream of fluctuating energy with a low steady flow followed by quick flooding. The Eocene clay shale is encountered at a depth of 12.5 m and was formed near a paleo-shoreline during a high stand of sea level 45 million years ago. The average properties of the soil layers are summarized in Figs. 1, 2, and 3. In Fig. 2, the graph describing the particle size shows two lines joining data points; these two lines are bounding the percent sand, with one line corresponding to the percent

Submitted: 1 October 2020; Published: 10 August 2021
Reference: Briaud J.L. (2021). 40 Years of Full-scale Infrastructure Testing at a National Geotechnical Experimentation Site: Sand Site. International Journal of Geoengineering Case Histories, Volume 6, Issue 3, pp. 25-53, doi: 10.4417/IJGCH-06-03-02

passing 4.75 mm and the other lines showing the percent passing 0.075 mm. This graph confirms that the deposit is a sand deposit down to about 12.5 m. The ground water level is found at a depth of 7.5 m.

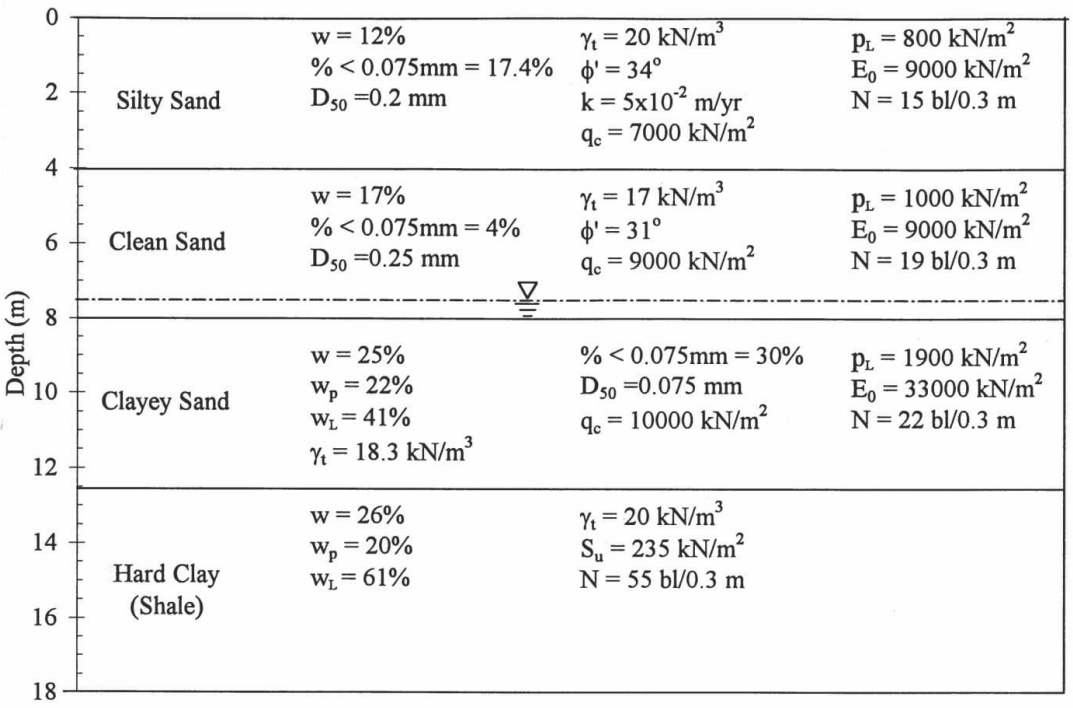


Figure 1. Stratigraphy of the NGES-TAMU sand site (Briaud, 1997).

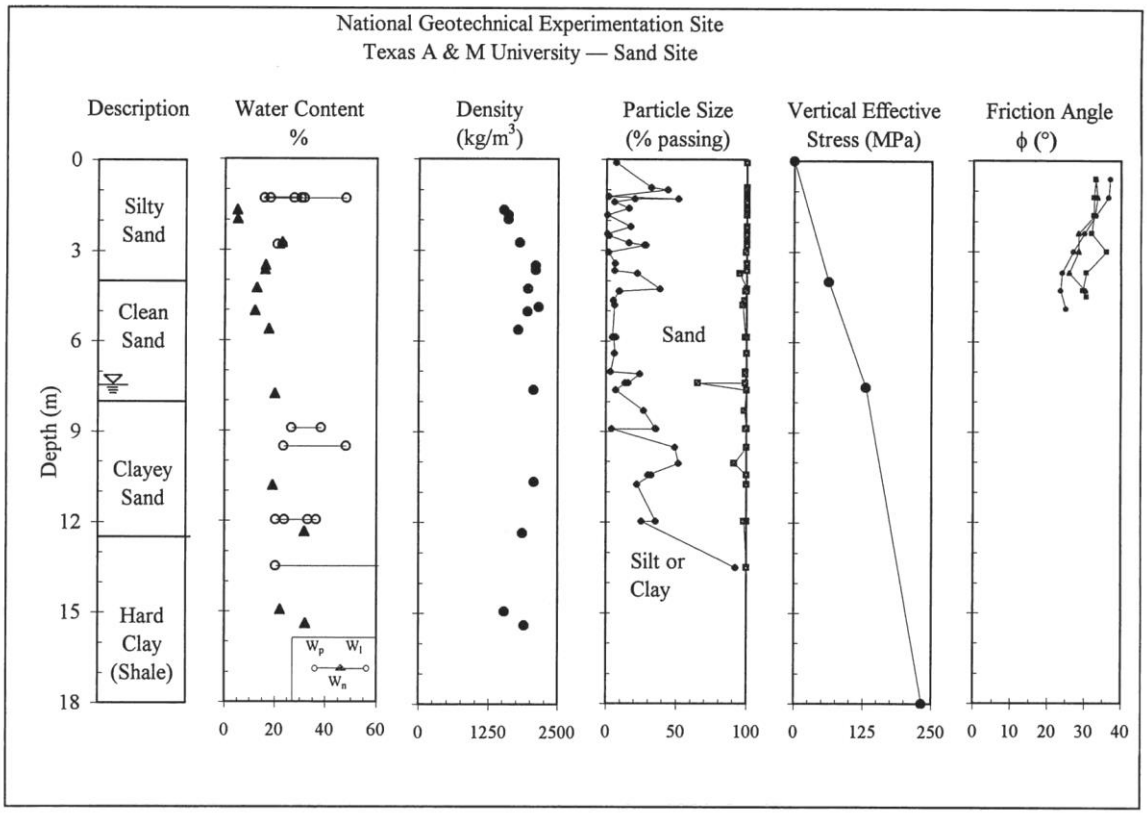


Figure 2. Laboratory test results (Briaud, 1997).

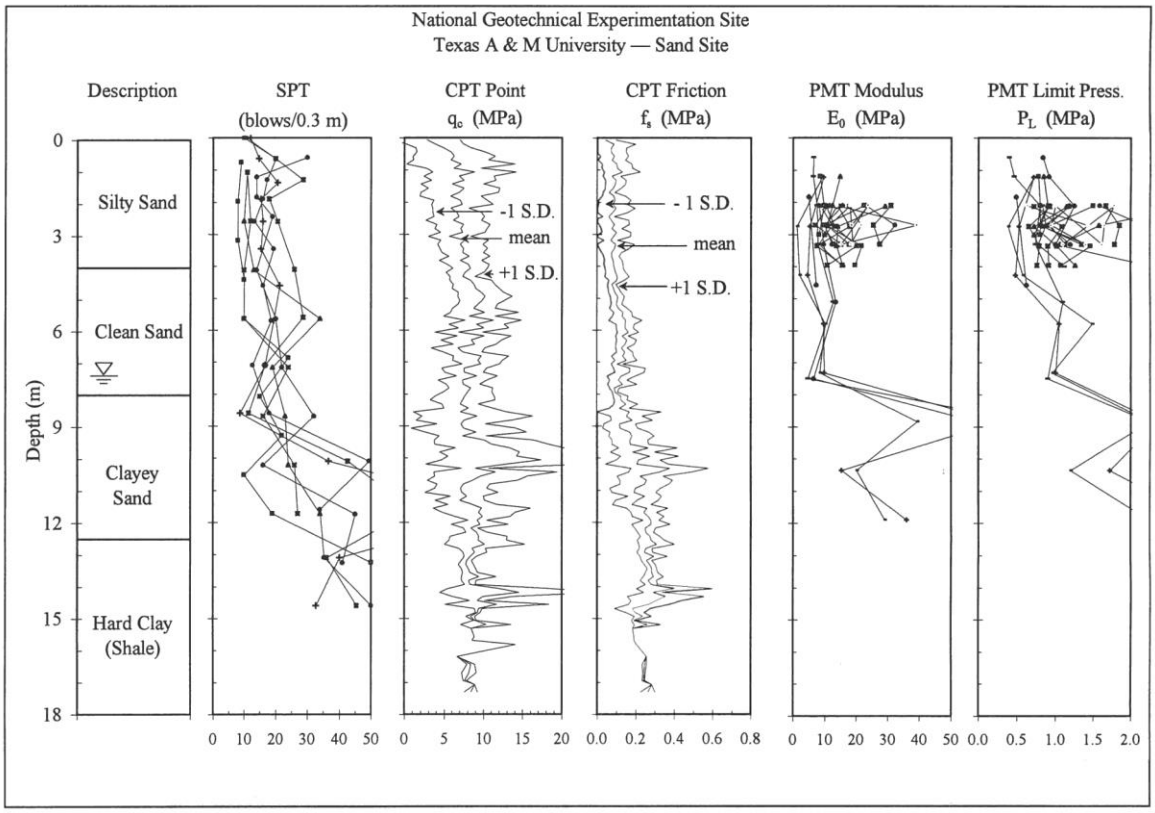


Figure 3. In-situ test results (Briaud, 1997).

BOX CULVERT WITHIN AN EMBANKMENT

This project started in 1982 and consisted of constructing a concrete box culvert, instrumenting it with pressure cells and recording the pressure generated by the fill placed on top of it and by a heavy truck passing over it (James et al., 1986). The inside dimensions of the culvert were 2.44 m wide, 2.44 m high, and 13.42 m long (Fig. 4). The roof and walls of the culvert were 200 mm thick and made of reinforced concrete. It was instrumented with 20 pressure cells, 12 on the top and 4 on each side, as well as strain gages in the concrete reinforcement. An embankment was built with the sand from the site in a direction perpendicular to the culvert main axis. Thus, the fill was a poorly graded red silty sand with 89 % finer than 0.425 mm (sieve no.40) and 8.3% finer than 0.075 mm (sieve no. 200).

The embankment was about 50 m long, had a top width of 3.66 m, and side slopes of 2 horizontal to 1 vertical. The thickness of the embankment was gradually increased from the bottom of the culvert up to 2.5 m above the top of the culvert. Measurements were taken for thicknesses of the fill on top of the culvert equal to: 0.2 m, 0.61 m, 1.22 m, 1.83 m, and 2.44 m. Also, for each one of those thicknesses a 330 kN eighteen-wheel tractor trailer truck was driven over the culvert (Fig. 5) while pressure cells and other instrument readings were recorded. The load on each of the two axles at the back of the truck was 108 kN and each axle had two groups of two tires for 27 kN per tire. The tire pressure was 550 kPa which means that the contact area was 0.0491 m^2. This area would be equivalent to a 0.25 m diameter circular imprint of the tire on the soil surface.

The pressure on the top of the culvert, given by the pressure cells, increased as the fill increased in height (Fig. 6). As can be seen, the scatter is not negligible but the trend matches the total vertical stress σ expressed as γz where γ is the soil total unit weight of 20 kN/m^3 and z is the depth of fill. This depth of fill refers to the thickness of the fill; it was zero when the fill level is near the bottom of the culvert, thus the pressure cells on top of the culvert only started to record pressure when the fill reached the top of the culvert. The pressure cell readings as the rear axle of the truck passed on top of the cells and for different depth of cover are shown in Fig. 7. Remember that the tire pressure was of the order of 550 kPa, yet the pressures on the cells placed on the roof of the culvert were much smaller than 550 kPa. In fact, they seemed to obey the stress distribution that one would have obtained from a bulb of pressure elastic approach (Briaud, 2013).

Indeed, for a 0.25 m diameter loaded area of the tire, as discussed above, the vertical stress increase at a depth of 0.20 m, or 0.8 times the diameter of the loaded area, was 0.44 times the pressure at the surface according to the elastic approach. This would be 0.44 x 550 kPa = 242 kPa while the maximum recorded pressure in that case was 190 kPa. At a depth of 0.61 m, the stress increase was 69 kPa—more than that given by the elastic approach for one tire (39 kPa), likely because of the overlap of stress bulbs between the two tires on one side of the axle. At a depth of 1.22 m, the vertical stress increase under the tires was insignificant. The horizontal pressure on the pressure cells mounted on the side walls of the culvert indicated pressures about two times higher than the active pressure and was likely induced by the compaction process (Fig. 8).

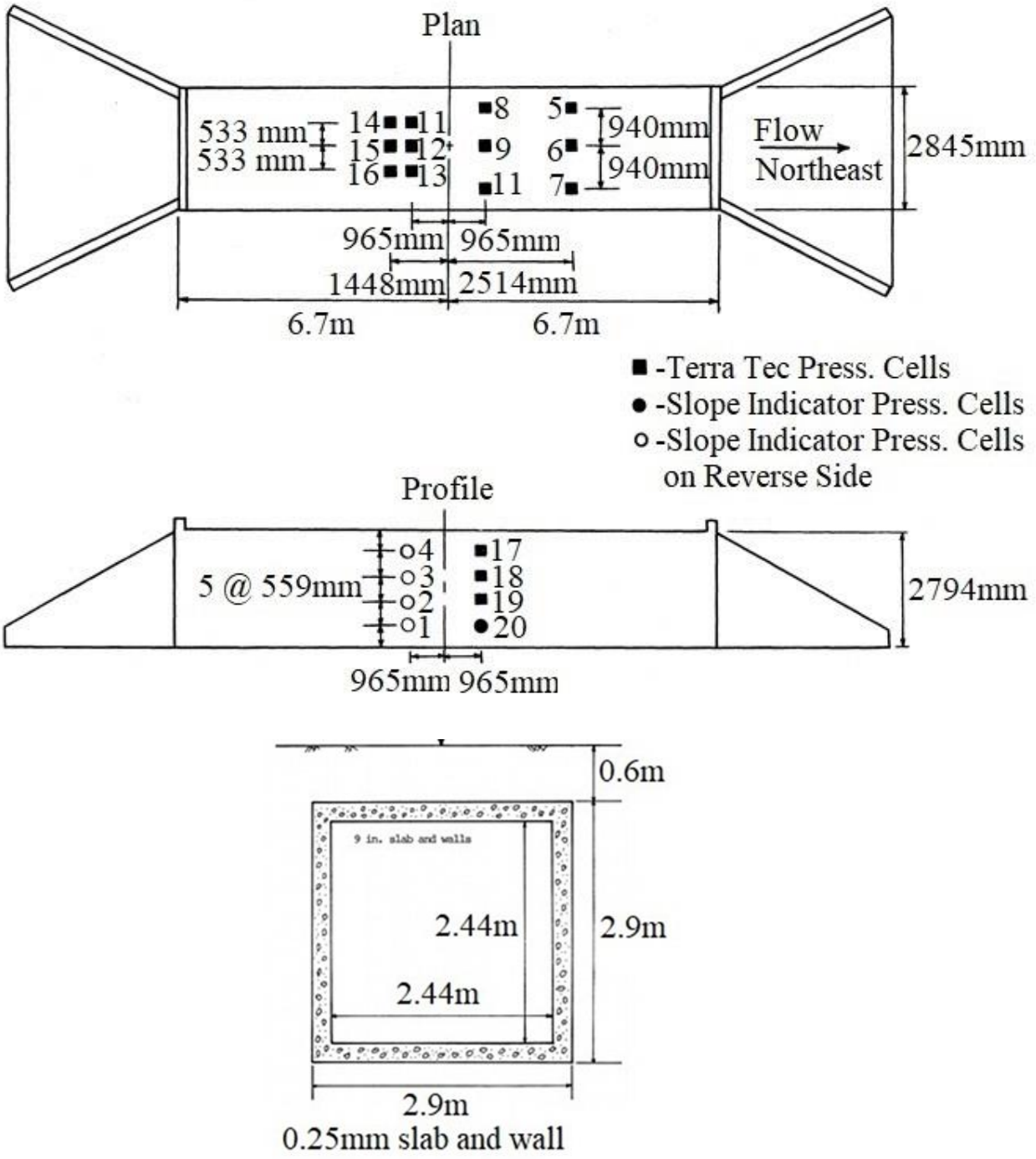


Figure 4. Culvert and location of pressure cells (after James et al., 1986).

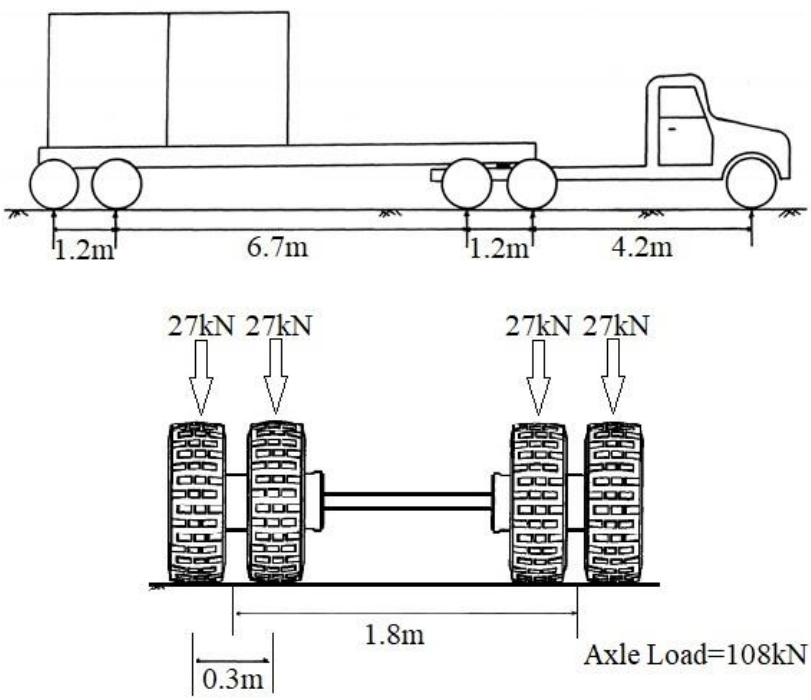


Figure 5. 330 kN tractor trailer truck used to load the culvert (after James et al., 1986).

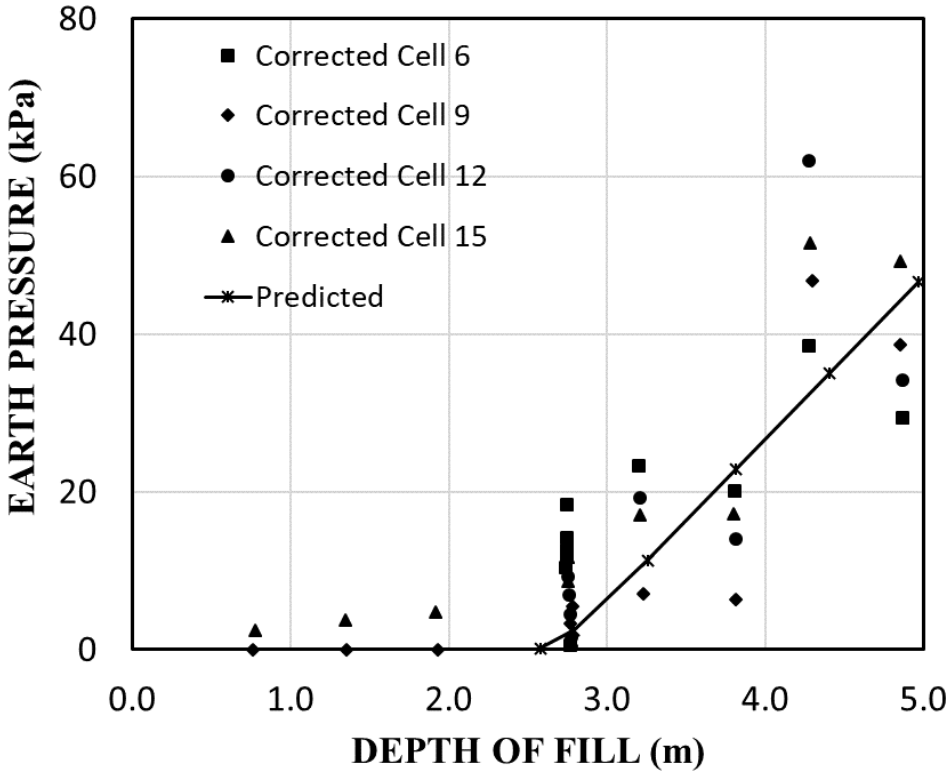


Figure 6. Pressure cell readings as a function of the fill height (after James et al., 1986).

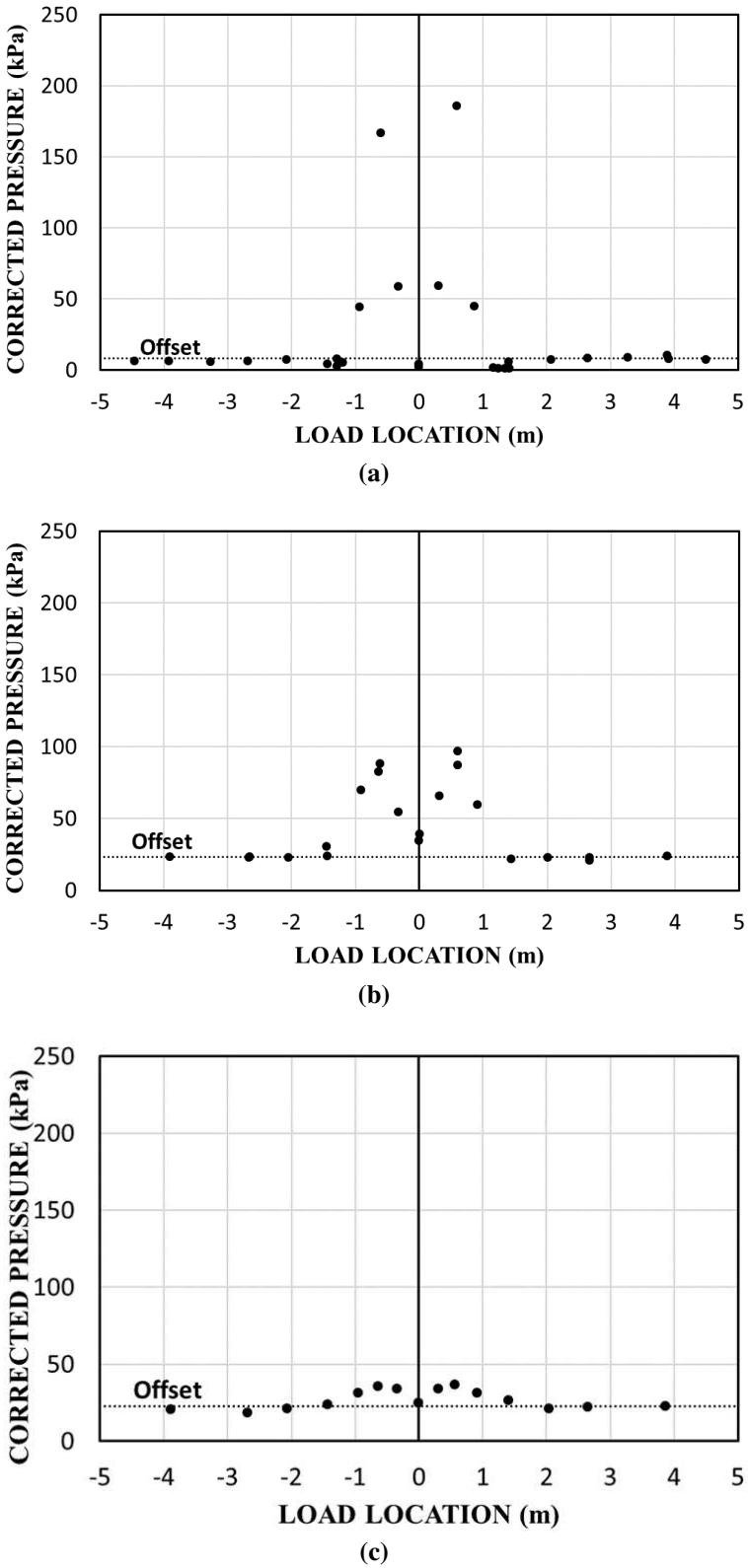


Figure 7. Pressure on top of the culvert for different heights of cover as the truck passes: a) 0.2 m of cover, b) 0.61 m of cover, c) 1.22 m of cover (after James et al., 1986).

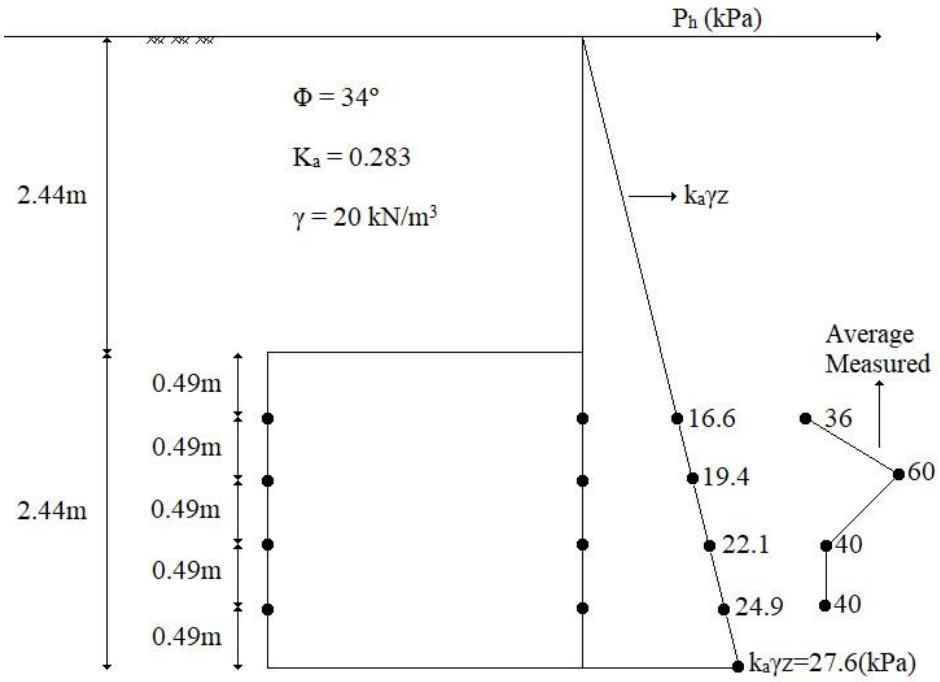


Figure 8. Pressure distribution on the side walls of the culvert.

SPREAD FOOTINGS OF VARIOUS SIZES

Five square footings were load tested in 1993 (Briaud, Gibbens, 1999; Briaud, 2007). The footing sizes were 1 m, 1.5 m, 2.5 m, 3 m, and 3 m; all were embedded 0.75 m into the sand. They were all pushed to 150 mm of penetration into the sand using the load test setup of Fig. 9. The load test results are shown in a normalized fashion on Fig. 10. The soil around and under the footings was instrumented to monitor the vertical soil movement versus depth by using tell tales and the lateral soil movement versus depth and versus lateral extent by using inclinometers on the side of the footings. The vertical movement with depth revealed that the zone of influence was shallower than given by elastic theories (i.e., bulbs of pressure); this was confirmed by the lateral measurements as well.

The width of the lateral zone of influence of the loaded footings was given by the inclinometers to be less than 2 times the footing width from the edge of the footing. The shape of the lateral movement vs. depth profiles never showed the existence of a shear slip surface as in the classical bearing capacity theory; instead, it showed a lateral bulging similar to the expansion of a pressuremeter probe. This is what led to the development of the PMT load settlement curve method for spread footings (Briaud, 2007). The load test results were also used to develop a long-term settlement prediction model. Indeed, some of the load steps were maintained for 24 hours while recording settlement vs. time (Fig. 11). The linearity of the data on a log-log plot led to the following model:

$$\frac{s}{s_1} = \left(\frac{t}{t_1}\right)^n \tag{1}$$

Where s is the settlement at time t, s_1 is the settlement at reference time t_1, and n is the long-term creep exponent. In Fig. 11, the time t_1 was chosen as one minute and the settlement s_1 was the settlement corresponding to the one-minute reading; the creep exponent can then be calculated as 0.02 and it matched the one found in special PMT creep tests at the site. Then the settlement at 50 years, for example, can be calculated from Eq. 1. These full-scale footing tests also gave the ultimate bearing pressure defined as the pressure corresponding to a settlement equal to 10% of the footing width. This ultimate pressure $p_{0.1B}$ was then correlated to the soil properties and gave:

$$p_{0.1B}(kPa) = 1.7\,p_L = 0.23\,q_c = 75N(bpf) \tag{2}$$

Where p_L is the pressuremeter limit pressure, q_c is the cone penetrometer point pressure resistance, and N is the Standard Penetration Test blow count in blows per foot. These correlations satisfy the measured values in this project with a range of + or – 8%.

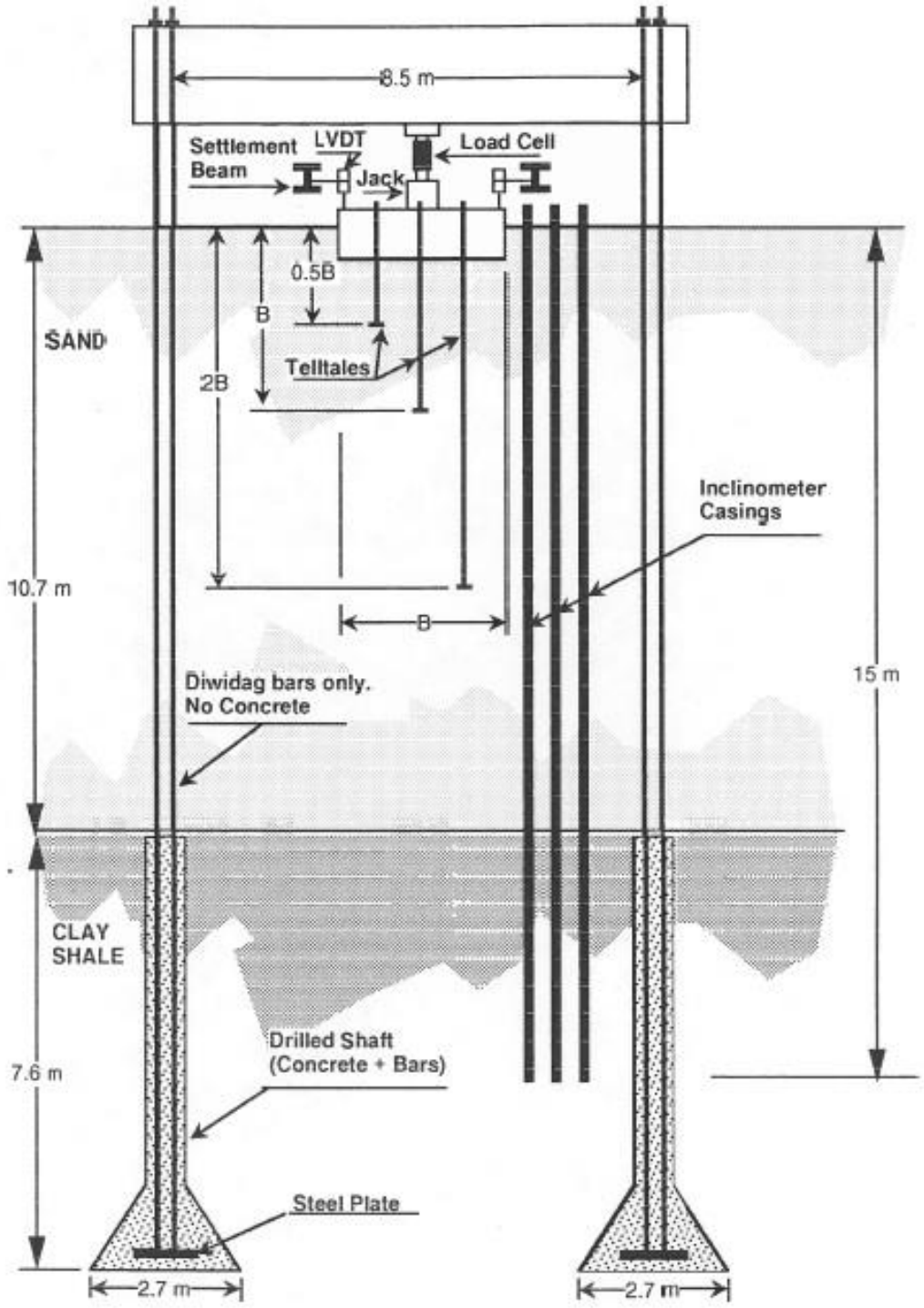


Figure 9. Load test setup for footing tests (Briaud, Gibbens, 1999).

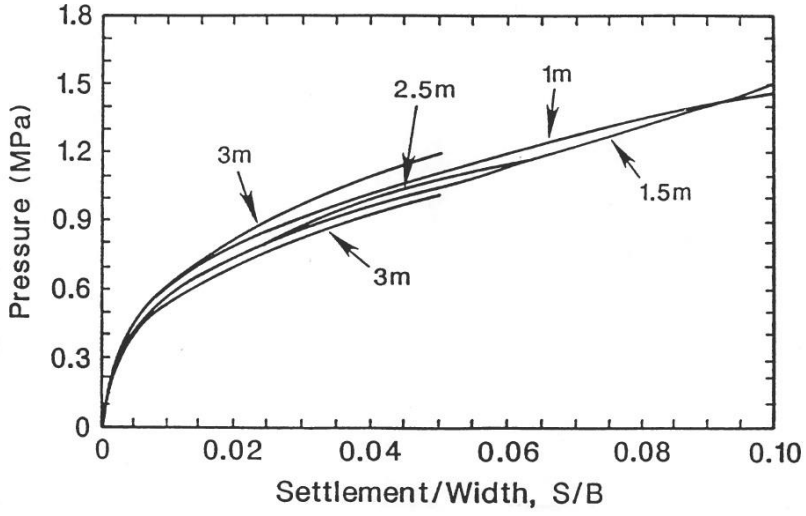


Figure 10. Normalized load test results for the five footings (Briaud, Gibbens, 1999).

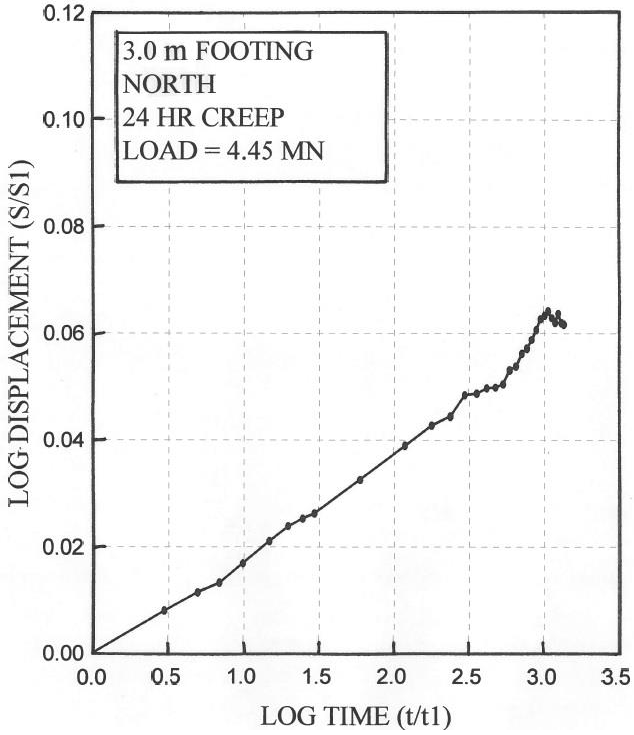


Figure 11. 24-hour creep test under constant load; t_1 is one minute and s_1 is the settlement corresponding to the one-minute reading (Briaud, Gibbens, 1999).

DETECTING DEFECTS IN DRILLED SHAFTS

Five 0.914 m diameter drilled shafts were built by A.H. Beck Foundation in 1991 (Ballouz et al., 1991, Briaud et al., 2002). The pile length and the size and location of defects are shown in Fig. 12. The defects were made of sealed sand bags attached to the reinforcing cage. Five Non-Destructive Testing (NDT) companies were invited to come and run their NDT tests and make blind predictions of the length of each pile as well as the location and size of the defects. The methods used were Sonic Echo (SE), Impulse Response (IR), Impedance Logging (IP), and Sonic Logging (SL). The success rate in predicting the length of the piles was gaged in three categories: within + or – 5%, within + or – 15%, and not within + or – 15%. The results are shown in Fig. 13.

The success rate in predicting the location and size of the defects was also gaged in three categories: good prediction, fair prediction, and poor prediction. Good prediction meant that the type of defect was well defined, and the location was within + or – 0.6 m. Fair prediction meant that the type of defect identified was ambiguous and the location was within + or - 1.8 m. Poor prediction meant the defect type and location was not detected. The results are shown in Fig. 14. During the process of predicting the defects, a number of defects were predicted to exist but did not actually exist according to the construction record; this is called a false negative. Fig. 15 shows the false negatives. Overall, the NDT techniques used in 1994 provided a reasonable estimate of the length of drilled shafts but did not give a reliable estimate of defects in drilled shafts.

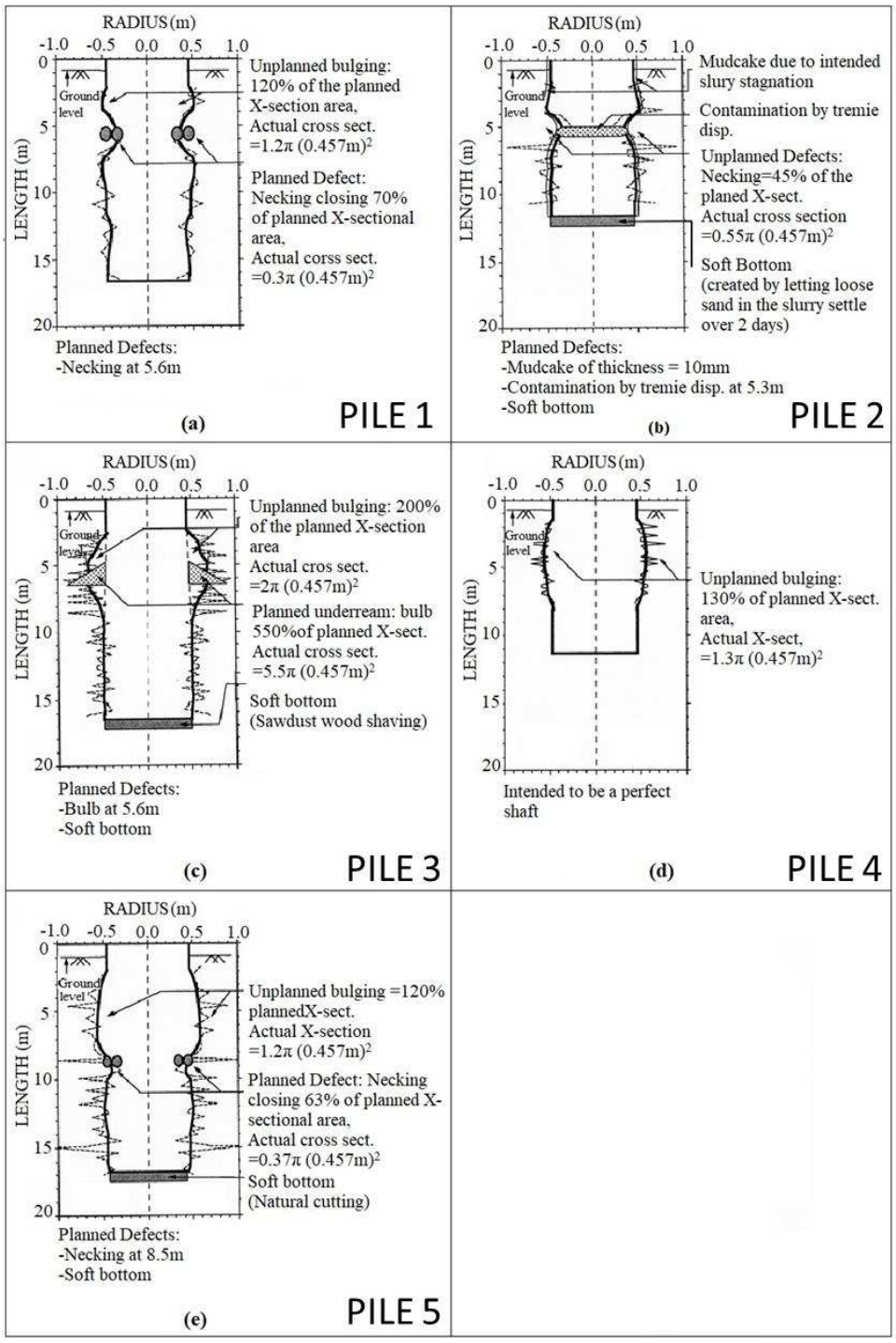


Figure 12. Five drilled shafts with planned defects (after Ballouz et al., 1991).

Site (1)	Pile Number (2)	Actual Length (m) (3)	ON SITE A (4)	ON SITE B (5)	ON SITE C (6)	ON SITE D (7)	ON SITE E (8)	SE C (9)	SE D (10)	SE E (11)	IR A (12)	IR B (13)	IR C (14)	IR D (15)	IL A (16)
SAND	1	16.6	●	○	●	◒	●	●	●	●	●	○	●	●	●
	2	11.6	●	●	●	●	●	●	◒	●	●	●	●	●	●
	3	16.5	●	○	◒	●	●	●	●	●	●	●	●	●	●
	4	11.4	-	-	-	-	-	-	-	-	-	-	-	-	-
	5	16.8	○	○	○	○	○	●	○	○	●	◒	○	○	○
CLAY	6	24.1	●	○	●	○	○	◒	○	○	◒	○	◒	○	●
	7	10.7	-	-	-	-	-	-	-	-	-	-	-	-	-
	8	12.2	●	●	●	◒	◒	●	●	●	●	●	●	◒	●
	9	10.4	●	●	◒	◒	◒	◒	●	◒	●	●	◒	●	●
	Percent Success		86%	43%	71%	50%	57%	86%	64%	64%	93%	64%	71%	64%	86%
	Average		61%					71%			73%				86%

On Site - Predictions made on site, the day of the test, before access to the PVC pipes was allowed.
SE, IR, IL - Final predictions made by Sonic Echo (SE), Impulse Response (IR), Impedance Logging (IL)
A,B, C, D, E -Letters identifying the predicting company
● - Length predicted within ±5%
◒ - Length predicted not within ±5%, but within ±15%
○ - Length not predicted within ±15%

Figure 13. Success rate for predicting the drilled shafts length (after Ballouz et al., 1991).

Site (1)	Pile No. (2)	ACTUAL DEFECTS: Type and Size (as % of Area) (3)	ACTUAL DEFECTS: Location from top (m) (4)	SONIC ECHO C (5)	SONIC ECHO D (6)	SONIC ECHO E (7)	IMPULSE RESPONSE A (8)	IMPULSE RESPONSE B (9)	IMPULSE RESPONSE C (10)	IMPULSE RESPONSE D (11)	SONIC LOGGING A (12)	SONIC LOGGING C (13)	IMPEDANCE LOGGING A (14)
SAND	1	Bulging (+20%) (U)	2.0 - 4.0	●	●	●	●	●	●	○	◒	◒	●
		Necking (-70%)	5.6	○	●	○	●	○	○	●	●	●	●
	2	Mud Cake (15 mm)	0 - 11.6	○	○	○	○	○	○	○	○	○	○
		Tremie Displ. (100%)	5.3	○	○	○	●	○	○	○	●	○	●
		Necking (-45%) (U)	5.0	◒	◒	●	●	◒	◒	●	○	○	○
		Soft Bottom (100%)	11.6	●	○	○	○	●	●	○	○	○	○
	3	Underream (+450%)	5.6	●	●	●	○	○	○	○	○	○	●
		Side Failures (Bulging +100%) (U)	3.0 - 8.0	●	●	●	◒	●	●	○	○	○	●
		Soft Bottom (Sawdust 100%)	16.5	○	○	○	○	○	○	○	○	◒	○
	4	Bulging (+30%) (U)	1.2 - 7.5										
	5	Necking (-63%)	8.7	○	○	○	●	◒	○	○	●	◒	●
		Bulging (+20%) (U)	3.0 - 8.0	●	●	●	◒	○	●	○	○	○	●
		Bulging (+20%) (U)	11.5 -14.0	◒	○	○	○	●	◒	○	○	○	●
		Soft Bottom (Cuttings 100%)	16.8	○	○	○	○	○	○	○	○	○	○
CLAY	6	Necking (-43%)	18.0	●	○	○	○	●	◒	○	●	●	●
		Soft Bottom (100%)	24.1	○	○	○	○	○	●	○	◒	●	○
	7	No Defect											
	8	Inclusion (-12%)	6.5	●	○	○	○	○	●	○	●	●	○
		Underream (+450%)	12.2	○	○	●	○	◒	○	○	○	○	●
		Soft Bottom	12.2	●	○	○	○	○	○	○	○	○	○
	9	Necking (-50%)	3.0	○	●	●	●	●	○	●	●	◒	●

● - Good Prediction: Type well defined and location within ±0.6 m
◒ - Fair Prediction: Type ambiguous and location within ±1.8 m
○ - Poor Prediction: Type and location undetected
(U) - Unplanned Defect
A, B, C, D, E - Letters identifying the predicting companies

Figure 14. Success rate for predicting the type and location of the defects (after Ballouz et al., 1991).

Site (1)	Pile No. (2)	Company A (3)	Company B (4)	Company C (5)	Company D (6)	Company E (7)
SAND	1		Cave-in (17.4 m)			
	2					
	3	Necking (6.0 m)	Necking (6.1 m) Bell (9.7 m)	Necking (12. 6 m)	Necking (7.3 m)	
	4			Necking (5.4 m)		Necking (5 m)
	5			Necking (4.8 m)		
CLAY	6	Bulb (3.2 m) Necking (9.5 m)	Bulb (2.7 m) Necking (10.4 m)	Defect (10.4 m)	Necking (4.3 m) Necking (10.4 m)	
	7	Bulb (2.3 m) Soft bottom	Small bulb near top	Soft bottom		
	8	Bulb (2.1 m)		Defect (2.6 m)	Bulb (2.7 to 3.7 m)	
	9	Soft bottom	Bulb (4 m) Necking (10 m)	Bulb (3.2 m)	Bulb (5.5 m)	

Figure 15. Predicted defects where none existed according to the construction records (after Ballouz et al., 1991).

STATIC AND DYNAMIC LOAD TESTING OF DEFECTIVE DRILLED SHAFTS

Some of the drilled shafts constructed with defects for the defect detection project were load tested by conventional static load testing with a reaction frame as well as load tested by Statnamic testing and by impact driving. Shaft #2 and Shaft #4 were first subjected to static load testing. Drilled Shaft #4 had been built under slurry with the best practice methods while drilled Shaft #2 had also been built under slurry but purposefully with very poor practice methods; the bentonite slurry was not desanded during drilling, the slurry was left in the open hole for three days before concreting the shaft, and the tremie was "burped" during the concrete pour. As a result of this intentionally poor construction, a 10 mm thick mud cake (measured by lateral sampling) was formed on the wall of the drilled shaft. Also, a 0.3 m thick cushion of loose sand had accumulated at the bottom of the open hole before the shaft was concreted.

Shafts #2 and #4 were load tested to a vertical displacement of 140 mm by applying a vertical load at the pile top and measuring the vertical displacement also at the pile top. The load settlement curves in Fig. 16 show that the load at 140 mm of settlement, or 15% of the shaft diameter, was 4200 kN for the well-constructed shaft and 1320 kN for the poorly-constructed shaft (or 3.18 times less). This demonstrates the critical importance of proper construction practices, which may induce uncertainties larger than those induced by the design methods themselves, and the need for construction quality control. The two shafts were instrumented with extensometers such that the point load was known at any time during the load tests. The load distribution indicated that there was a major difference in the friction load but little difference in the point resistance load, at least at large displacements; at 140 mm of vertical displacement, the point resistance was 1000 kN for Pile 2 and 830 kN for Pile 4. Therefore, the loose sand cushion was likely recompressed and transferred the total point capacity at a large displacement, but the friction load never recovered. The drilled shafts were also tested by Statnamic testing and by pile driving. The static capacities were back calculated from these dynamic tests and the results were mixed; it may not be fair to mention those results here, however, as such methods have improved since the tests were performed (1991). Nevertheless, the details of the results can be found in Briaud et al. (2000) and in Ballouz et al (1991).

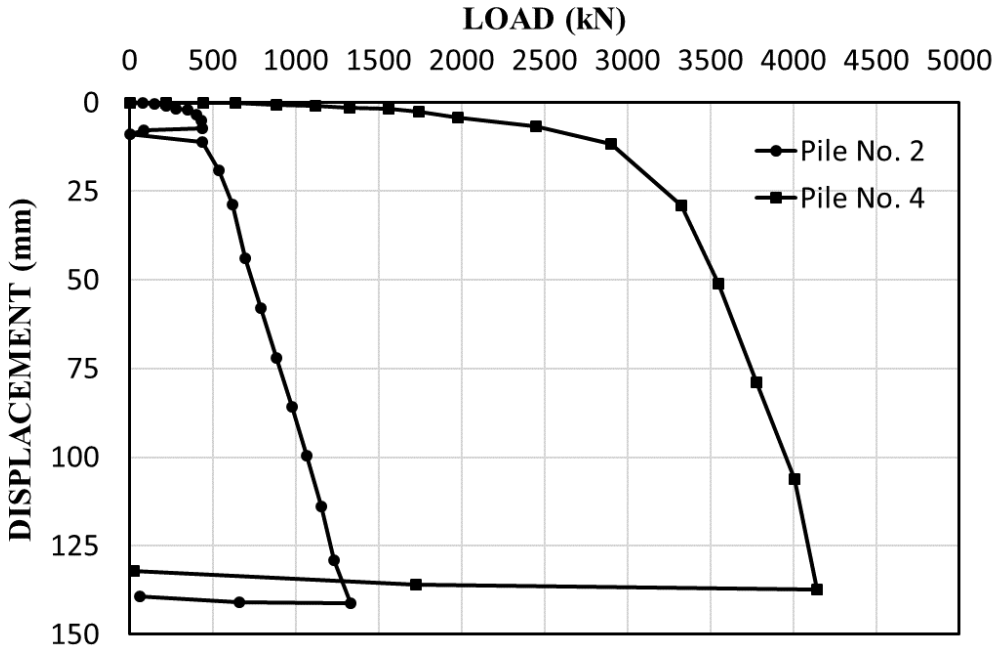


Figure 16. Load vs. displacement curves for Bored Piles #2 and #4 (after Briaud et al., 2000).

A 10 M HIGH - 50 M LONG TOP DOWN ANCHORED RETAINING WALL

This 1990 project was a team effort between the Schnabel Foundation, FHWA, and Texas A&M University (Chung, Briaud, 1992, Kim, Briaud, 1992). The wall was a tieback soldier pile and lagging wall (Fig. 17). The H-piles were 9.15 m long with a spacing of 2.4 m center to center and the excavation wall height was 7.62 m. Half of this 50-m long wall had one row of anchors at a depth of 2.75 m and the H piles were HP 10 X 57 soldier piles; the other half had two rows of anchors at a depth of 1.8 and 4.9 m and the H piles were HP 6 X 25 soldier piles. The anchors were inclined downward at 30° with the horizontal and had a 2.4-m spacing (Fig. 17). Together with the wall, the anchors applied an average horizontal pressure against the soil of 20 kN/m^2. Eight of the 22 soldier piles were instrumented with about 450 vibrating wire strain gauges for bending moment and axial-load determination. Furthermore, 19 inclinometer casings were installed for wall and soil mass movement. The water table was at the bottom of the excavation.

Figs. 18, 19, and 20 show the average results for the section of the wall with two rows of anchors. Fig. 18 shows the horizontal deflection profile at the end of construction, Fig. 19 shows the bending moment profile, and Fig. 20 depicts the vertical load in the soldier piles. The same results are shown for the section of the wall with the one row of anchors in Figs. 21, 22, and 23. One of the many lessons learned from this project was that to limit the horizontal deflection of a tieback wall, the wall must have good vertical capacity. Indeed, such walls are subjected to significant downdrag from the retained mass (Figs. 20, 23), which is likely to induce settlement of the facing. This settlement generates rotation around the back of the anchors and an associated horizontal movement even if the anchors properly resist the horizontal load. Another outcome was the development of P-y curves, which do well in predicting the bending moment distribution in the soldier piles. The P-y curve approach was unable to accurately predict the deflection; only the finite element method could accomplish a good fit.

Other case histories were analyzed to generate a relationship between the horizontal pressure coefficient K and the deflection at the top of the wall normalized by the wall height (Fig. 24). The pressure coefficient K is defined here as the mean pressure on the wall divided by the vertical effective stress behind the wall at the bottom of the excavation. The value of K for the Terzaghi and Peck constant pressure diagram for tieback walls in sand (0.65 K_a) corresponds to a K value of about 0.2 in Fig. 24. Note that tieback walls are one of the few retaining wall cases where the engineer can choose a deflection-based design; in fact, the anchor load can be chosen to achieve a desired deflection via a chart, as shown in Fig. 24, for example. Note that this chart is limited to tieback walls with proper vertical capacity.

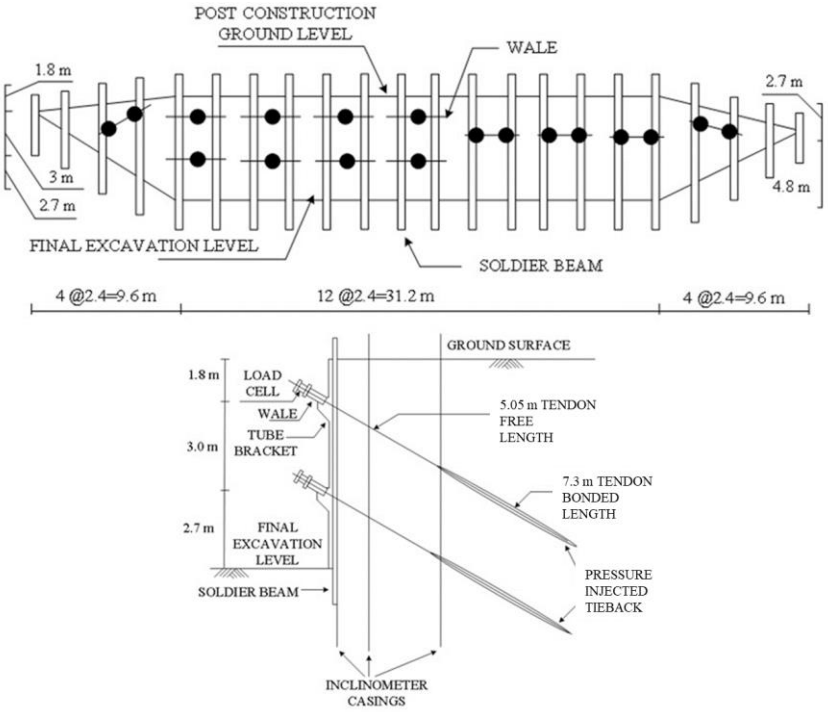


Figure 17. Tieback soldier pile and lagging wall (Chung, Briaud, 1992).

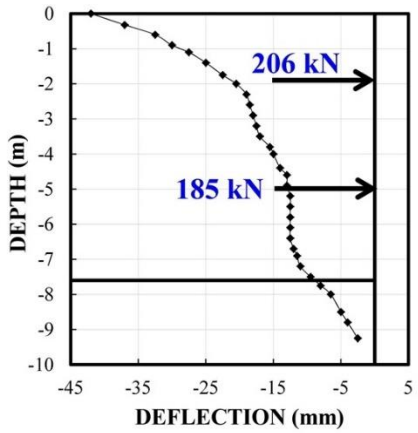


Figure 18. Wall deflection profile at end of construction for two rows of anchors (after Chung, Briaud, 1992).

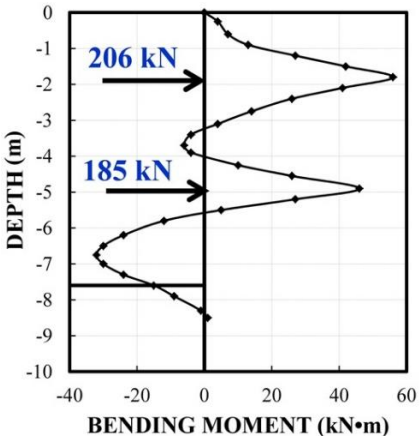


Figure 19. Wall bending moment profile at end of construction for two rows of anchors (after Chung, Briaud, 1992).

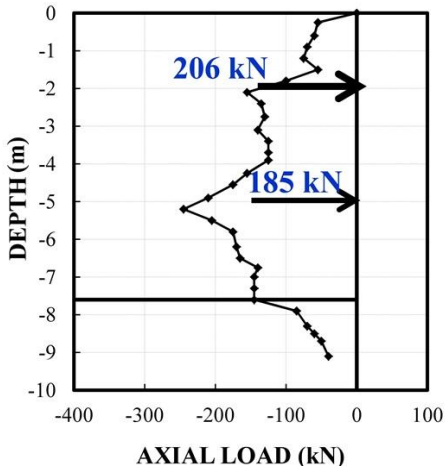


Figure 20. Wall vertical load at end of construction for two rows of anchors (after Chung, Briaud, 1992).

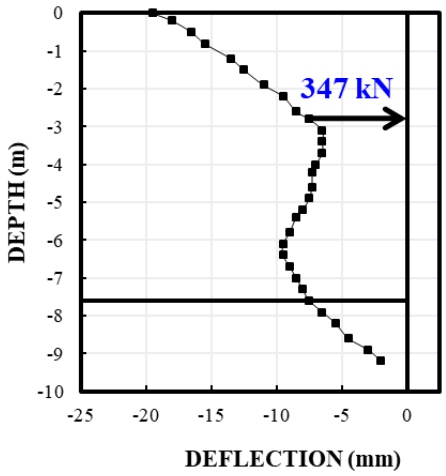


Figure 21. Wall deflection profile at end of construction for one row of anchors (after Chung, Briaud, 1992).

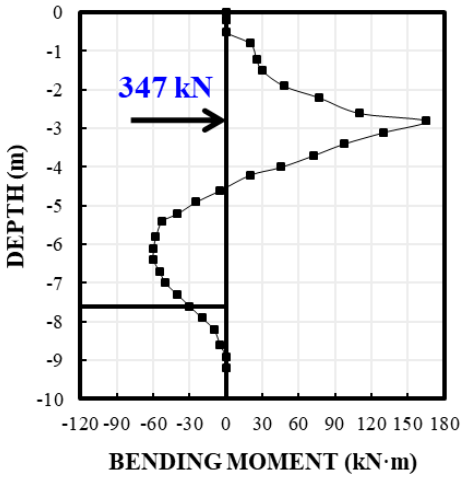


Figure 22. Wall bending moment profile at end of construction for one row of anchors (after Chung, Briaud, 1992).

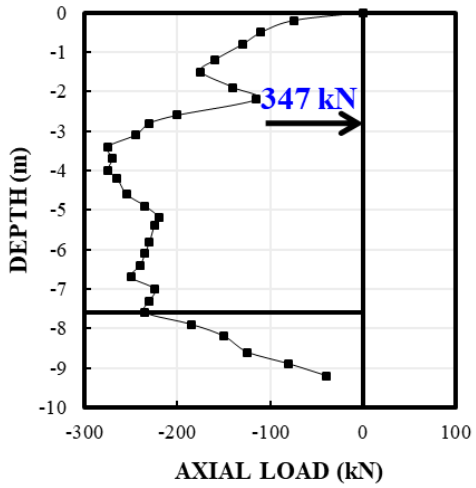


Figure 23. Wall vertical load at end of construction for one row of anchors (after Chung, Briaud, 1992).

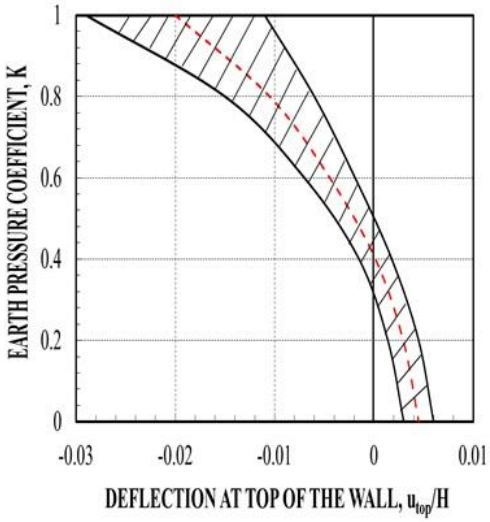


Figure 24. Earth pressure coefficient for pre-stressed anchored walls with proper vertical capacity (Briaud, 2013); positive deflection refers to movement towards the excavation, while negative deflection refers to movement of the wall into the retained soil.

A 7.5 M HIGH – 40 M LONG TOP DOWN DEEP-SOIL-MIXING RETAINING WALL

Following the tieback wall project, a new type of top down retaining wall called a VERT wall was built and tested very close to the tieback wall. This new type of wall was a deep soil mixing wall built by drilling several rows of soil-cement columns down to the depth of soil to be retained. A full scale 10 m high VERT wall was constructed with 0.91 m diameter soil cement columns (Briaud et al., 2000); the other dimensions of the wall are shown in Fig. 25. The columns were built using deep soil mixing equipment and a soil-cement ratio by weight of about 0.2. Over two thirds of the columns, a 1 m thick relieving platform was constructed using the overflow from the drilling process (Fig. 25(c)). This platform was unreinforced and was a thick slab of soil cement mixture. Once the soil-cement mixture had cured, excavation proceeded in one step.

To study the behavior of this new wall type, instruments were installed in and around the wall, including inclinometers, vertical extensometers, horizontal extensometers, and survey targets. The 28-day strength of the soil-cement mixture averaged 2180 kPa with a minimum of 1400 kPa. On 12 May 1998, 21 days after the soil-cement drilling process ended, the excavation started. The excavation was completed, and all the surcharges were built up on 27 May 1998. At that time, the maximum horizontal deflection of the wall was 14 mm (Fig. 26); the global wall movement is shown in Fig. 27. On 12 January 2000, or 595 days later, these deflections had increased by 78% to 25 mm. The plot of log deflection in mm versus log time in days was approximately linear.

One of the lessons learned was that a platform on top of the columns is critically important since the platform provides some restraint and makes the wall behave more as a block. The columns tend to deflect a lot more without the platform. This was demonstrated because one third of the wall did not have a platform (Fig. 25). Another lesson learned was that reinforcement (e.g., a vertical H beam) is needed in the front row of columns to better resist the bending moment. Overall, this new wall behaved comparably to the tieback wall next to it.

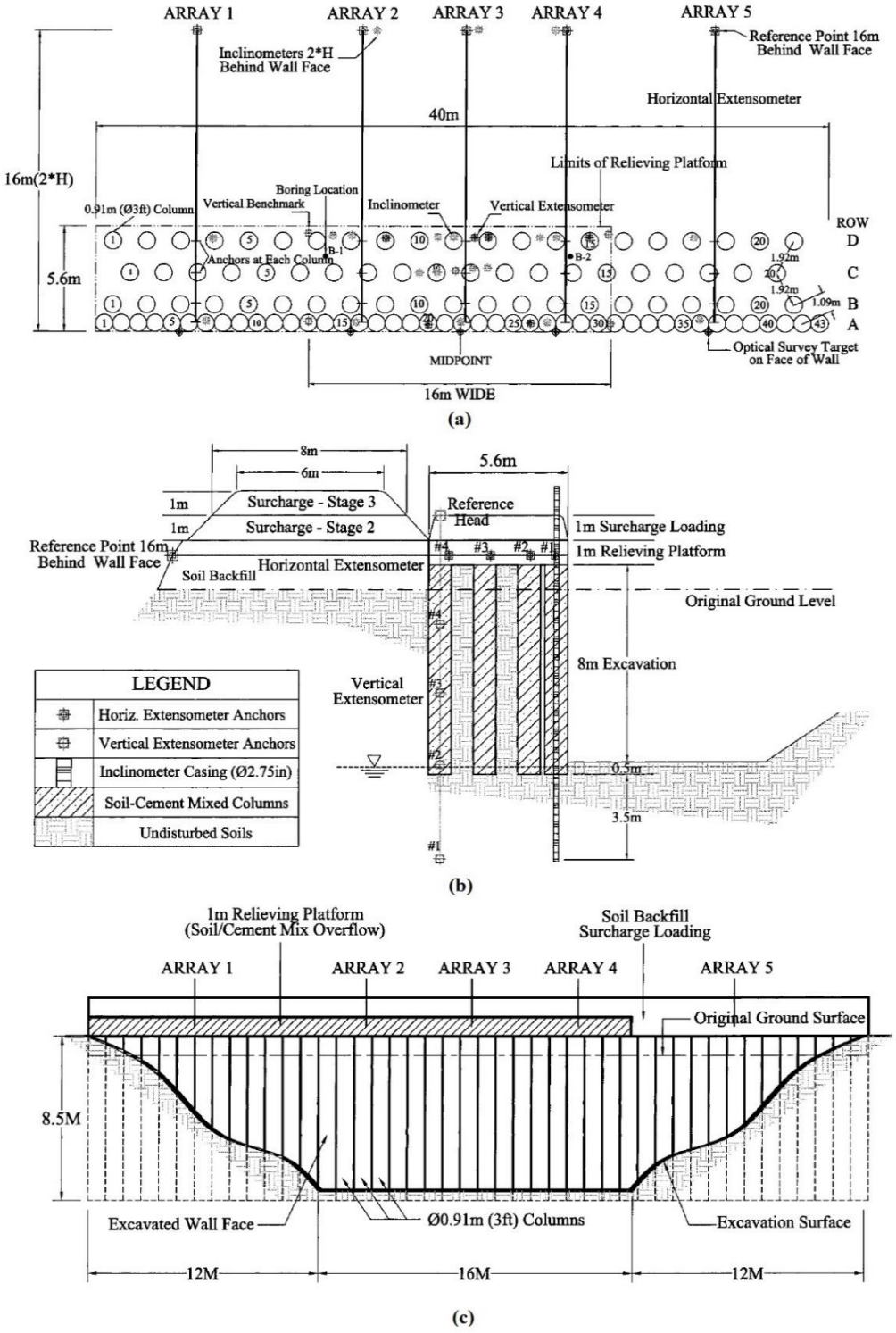


Figure 25. VERT wall a) plan view, b) cross section, c) front view (Lee, Briaud, 1999).

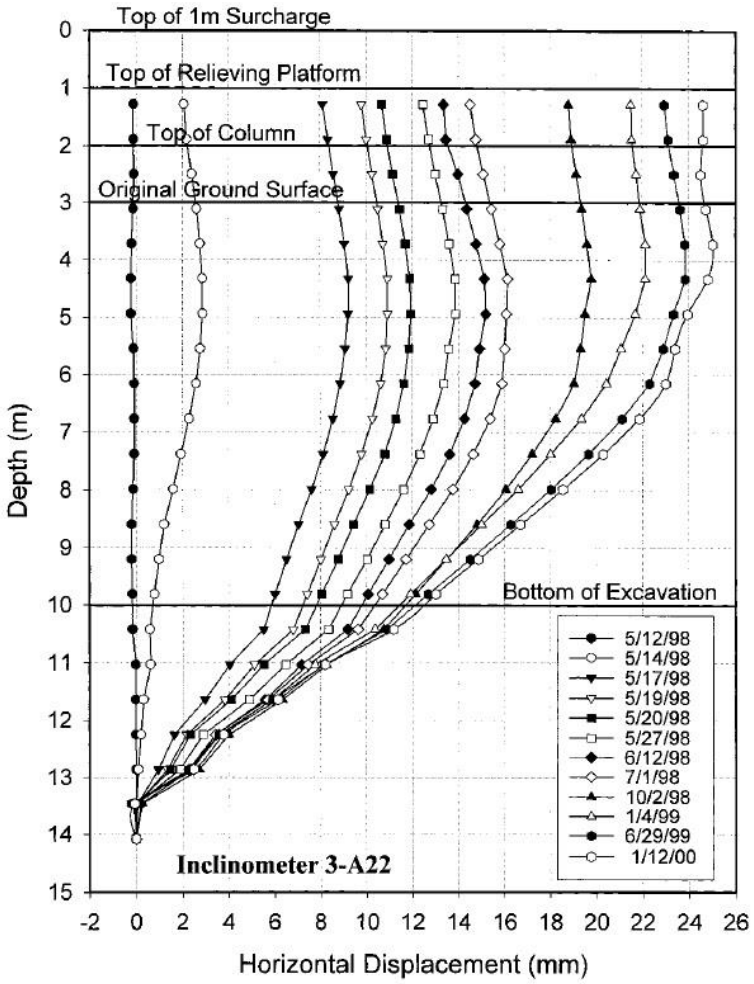


Figure 26. Horizontal movement of the center of the front of the wall: Array 3 with platform (Lee, Briaud, 1999).

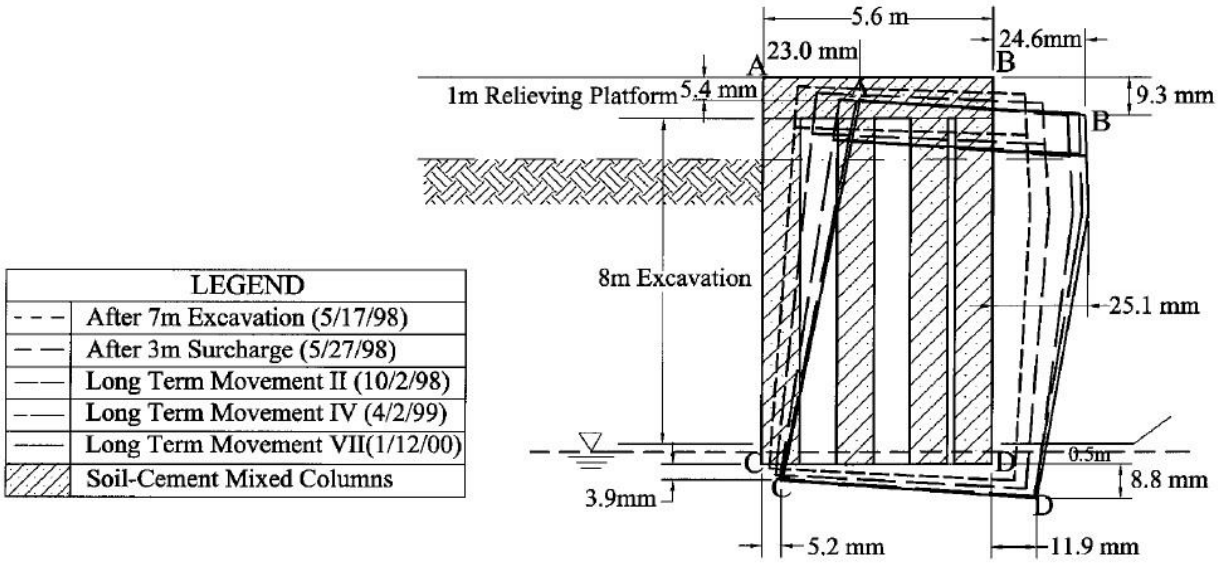


Figure 27. Mass movement of the wall block (Lee, Briaud, 1999).

POST GROUTED DRILLED SHAFTS – SYNCHROPILE

This 2005 project was sponsored by Synchropile to evaluate the increase in capacity due to post grouting of the drilled shaft bottom in sand (King et al., 2009, 2015). It consisted of building three drilled shafts: one post grouted drilled shaft (PGDS), one PGDS with a bottom O'Cell, and one regular drilled shaft without post grouting. All three drilled shafts were load tested to failure. The shafts were instrumented and had a 0.76 m nominal diameter and a length of 10 m. During the post grouting, the grout pressure reached 2000 kPa and the top of the shaft moved up about 15 mm. The load tests were carried out in general accordance with the quick load procedure of ASTM D1143. The load-deflection curves of Fig. 28 show that the ultimate capacities for the conventional and the PGDS drilled shaft are 2937 kN and 4116 kN, respectively. This represents an axial load capacity increase of 40.1%. Similarly, in Fig. 28, the axial loads required to produce a 25 mm top settlement are compared; they are 2090 kN and 3380 kN for the conventional and the PGDS drilled shafts, respectively. This shows that for a top deflection of 25 mm, an axial load of about 62% higher could be used for the PGDS as compared to the conventional drilled shaft. This is due to the fact that the post grouting process prestresses the drilled shaft against the soil, thereby limiting the amount of movement necessary to engage the soil response.

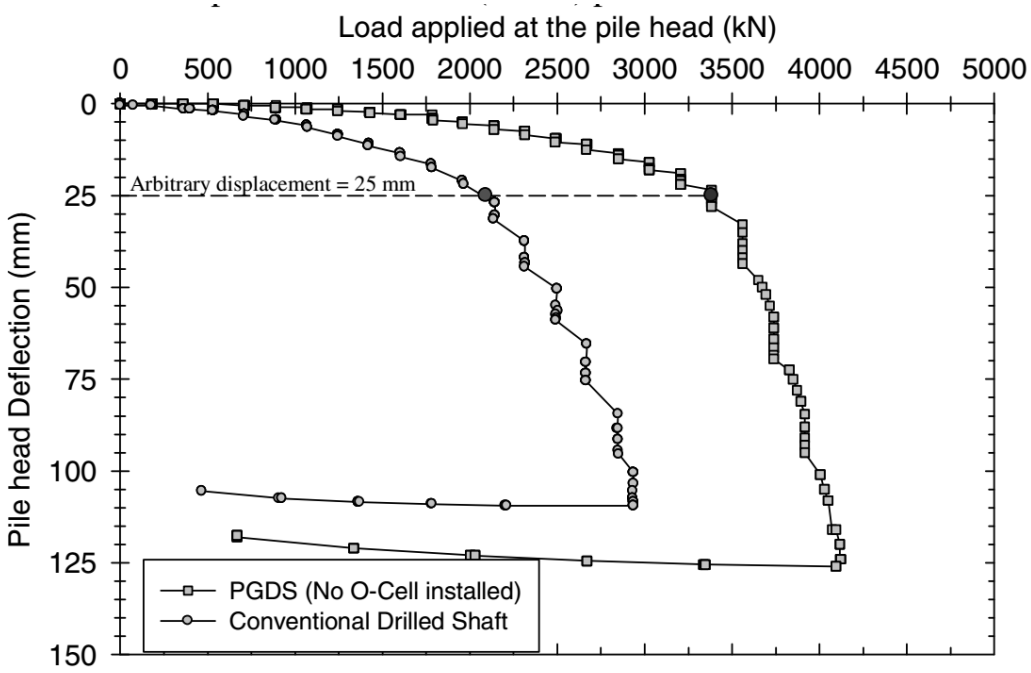


Figure 28. Load settlement curve for conventional and post grouted drilled shaft (King et al. 2015).

VIBRO-DRIVEN STEEL PILES

In 1997, 24 piles were driven with a vibrating hammer and subsequently load tested to failure to evaluate and possibly develop methods to predict the pile capacity based on the measurements made during the vibro-driving process (Bossher et al., 1998). The hammer was an ICE 416L with a total weight including the clamp of 44 kN, a frequency of 26.7 Hz, and an amplitude varying from 6 to 19 mm. Soil borings were drilled and confirmed the stratigraphy except for a stiff clay layer from 6.7 to 8.2 m. There were 12 H piles with embedment lengths of 5.1 and 8.1 m; a web height of 150, 200, and 250 mm; and 12 open-ended pipe piles with embedment lengths of 5.1 to 8.1 m and diameters of 170, 220, and 270 mm. The soil plug was measured in the open-ended pipe piles after driving and had a length varying from 1.25 to 2.55 m above the pile point with an average of 1.6 m; therefore, the pipe piles did plug during driving. The H piles did not plug.

Seventeen 13.8 m long H piles were also driven to provide a reaction for the load on the test piles. The piles were instrumented to monitor various parameters during driving, including accelerometers and strain gages at the top and bottom of the piles. The vibrating hammer was also instrumented with accelerometers on the bias mass and on the eccentric mass. Four months after driving, the load tests were performed according to the ASTM standard. The maximum load applied in the load tests ranged from 71 to 552 kN, and the maximum vertical movement varied from 25 to 75 mm. During driving, the penetration

rate was recorded. Note that over the first 3 m of penetration, the rate of penetration was controlled by the crane to maintain equilibrium of the vibratory hammer and not by the soil resistance. At that point, the crane control was released, and the rate was controlled by the soil resistance.

Fig. 29 shows the rate within the last 0.5 m of penetration vs. the ultimate capacity of the pile defined as the load reached at a displacement equal to 1/10th of the pile diameter in the static load test. Note that the penetration rate profile was sometimes erratic at the end of vibrating; this makes the case for using the end of re-vibrating to improve upon the predictions. Nonetheless, the trend is as expected with a decrease in capacity as the penetration rate increases, but the plot exhibits quite a bit of scatter. The Briaud Tucker method, meant to calculate the ultimate capacity of impact driven piles in sand on the basis of SPT blow count (Briaud, 2013), was used and compared well with the measured data after applying a 0.75 reduction factor for vibro-driven piles. Thus, it seems reasonable to propose that:

$$R_{uBT}\,(\text{vibro-driven}) = 0.75\ R_{uBT}\,(\text{impact driven}) \qquad (4)$$

where R_{uBT} (impact driven) is the ultimate static capacity of the impact driven pile calculated according to the Briaud-Tucker SPT method and R_{uBT} (vibro-driven) is the ultimate capacity of the same vibro-driven pile. This correlation requires further verification and can only be used for the first estimate.

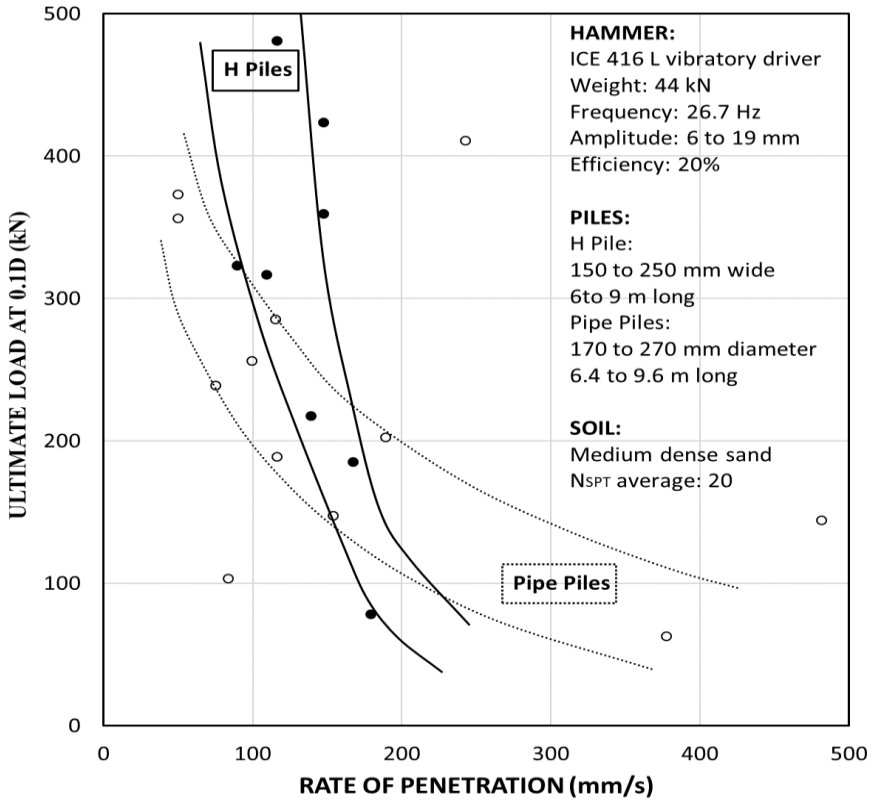


Figure 29. Ultimate pile capacity (D/10 criterion) vs. vibration rate of penetration (after Bossher et al., 1998).

HORIZONTAL LOAD ON DRILLED SHAFT BEHIND MSE WALL

Drilled shafts are sometimes constructed within the reinforced zone of Mechanically Stabilized Earth (MSE) walls, as in the case of overpass bridges where the drilled shafts carry the bridge deck or traffic signs. These drilled shafts may be subjected to horizontal loads and pushed against the front of the wall. This project was designed to study the interaction between the drilled shaft and the MSE wall and develop design guidelines (Briaud et al., 2015).

A 2.3 m high instrumented MSE wall was constructed and a 0.6 m diameter drilled shaft was placed behind the facing of the wall, with a clear spacing between the drilled shaft and the panel of the wall equal to 0.6 m (Figs. 30 and 31). The 5.5m long

drilled shaft was embedded 2.3m below the bottom of the MSE wall in medium dense sand, with the next 2.3 m being in the MSE wall backfill. The MSE wall backfill was a compacted uniform medium dense sand with a friction angle equal to 27.5 degrees; this clean uniform backfill is different from the native sand at the site. The drilled shaft was loaded horizontally to 0.15m of displacement while recording all instruments.

The data collected included the measurement of the horizontal load, the horizontal movement of the drilled shaft, the horizontal movement of the wall in front of the drilled shaft, and the pressure on the wall in front of the drilled shaft and on the drilled shaft. In addition, numerical simulations were conducted using FLAC 3D. All components of the MSE wall-drilled shaft system were simulated. The simulations were first calibrated against the full-scale experiment. A parametric study was then performed to identify the influence of each parameter on the MSE wall reinforcement. The load on the drilled shaft vs. the horizontal displacement of the drilled shaft, as well as the load on the dilled shaft vs. the horizontal displacement of the wall in front of the drilled shaft, are shown in Fig. 32.
It was found that at the maximum horizontal displacement in the horizontal load test, the maximum pressure on the drilled shaft was consistent with the calculated ultimate bearing capacity of the sand wedge between the drilled shaft and the MSE wall panel. This ultimate bearing capacity was calculated by assuming that the drilled shaft was a vertical strip footing with a width equal to the drilled shaft diameter. Based on the experiments and the simulations, MSE wall design guidelines were proposed. Among these guidelines is the inclusion of an additional pressure diagram $\Delta\sigma_s$ (Fig. 33) due to the design load on the drilled shaft; this additional pressure diagram is triangular and is to be resisted by the MSE wall reinforcement. The maximum pressure $\Delta\sigma_{s(max)}$ at the top of the diagram depends on the horizontal load H_o on the drilled shaft, the diameter B of the drilled shaft, the height h of the wall, and on the clear distance D between the drilled shaft and the front of the MSE wall (Fig. 33).



Figure 30. Construction of the MSE wall.

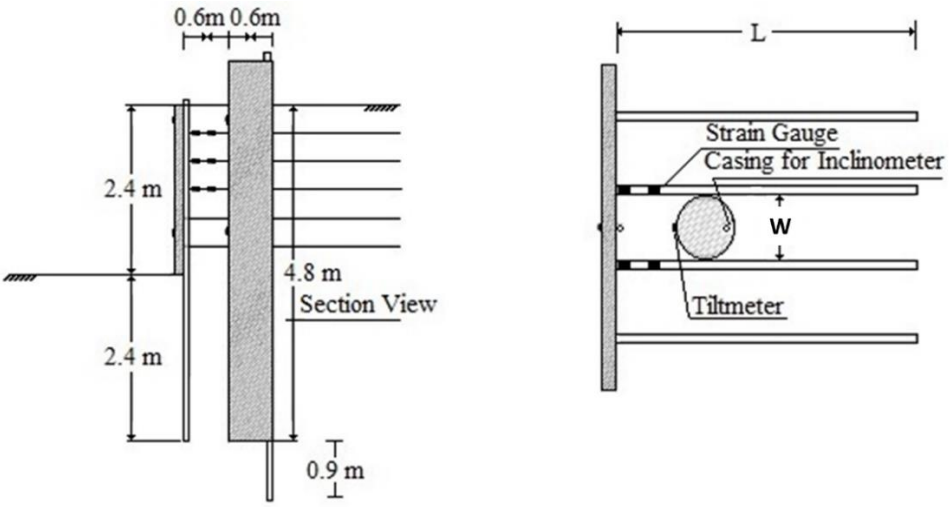


Figure 31. Setup and dimensions.

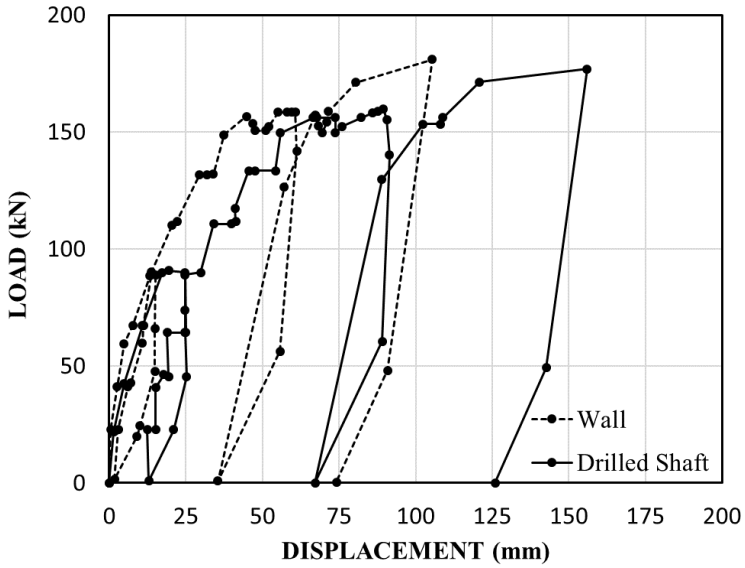


Figure 32. Measured load vs. displacement results for the drilled shaft and for the wall.

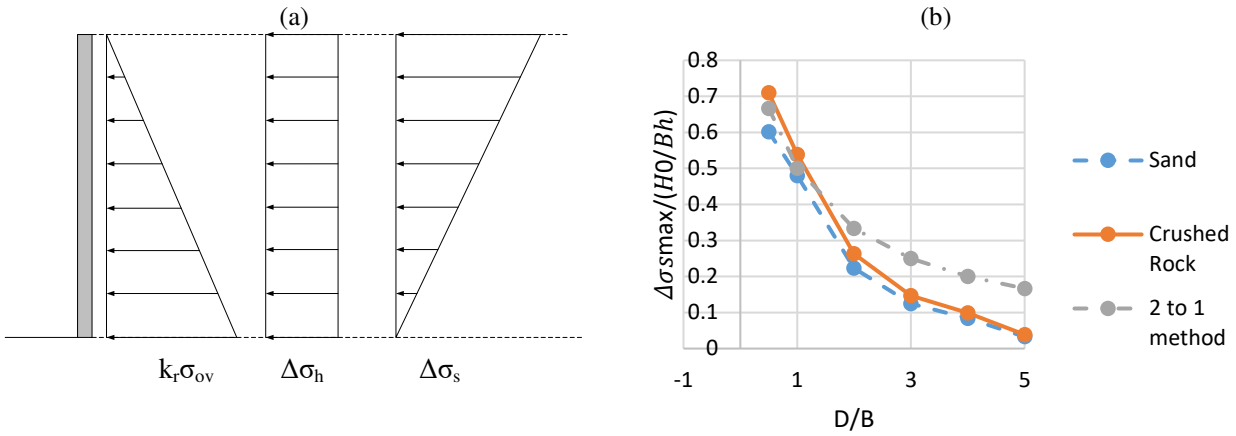


Figure 33. Recommended pressure diagram for drilled shaft behind MSE wall (Briaud et al., 2015): (a) pressure diagrams, (b) obtaining Δσsmax, where: k_r is the coefficient of earth pressure used for MSE walls (Briaud, 2013), σ_{ov} is the vertical stress at depth z below the ground surface, $\Delta\sigma_h$ is the increase in horizontal stress due to any surcharge applied at the top of the wall, $\Delta\sigma_s$ is the increase in horizontal stress due to the horizontal load on the pile, Δσsmax is the maximum pressure at the top of the inverted triangular diagram in (a), H0 is the horizontal load on the pile, B is the pile diameter, h is the height of the wall, and D is the clear horizontal distance between the front edge of the pile and the wall panel.

TRUCK IMPACT ON BARRIER ON TOP OF MSE WALL

Barriers that are built to redirect errant vehicles save lives. These barriers are typically attached to posts driven in the soil on the side of the road or tied to the deck for bridges; these two options, however, are not possible on top of MSE walls. Instead, MSE wall traffic barriers must be tied to a moment slab which provides resistance because the vehicle has to lift the moment slab up during the impact (Fig.34). The question in this case is how wide must the moment slab be, and how much load is transferred to the wall reinforcement? To solve this and develop associated design guidelines, a series of full-scale crash tests were performed at the National Site as well as via numerical simulations.

Reported here is the test for the largest truck. The MSE wall was built by first excavating and then building the wall from the bottom of the excavation up so that the top of the wall would end up at the level of the ground surface. The MSE wall was 3 m high from the bottom of the wall to the roadway level, and the horizontal reinforcement strips were 3 m long. The top of

the barrier was 1.07 m above the roadway level and the moment slab was 2.1 m wide (Fig. 34). The MSE wall backfill from the bottom of the wall to the bottom of the moment slab was compacted clean uniform sand; the mean grain size D_{50} was 0.51 mm, the in-place dry unit weight was 17.5 kN/m3, the in-place water content was 2%, the direct shear friction angle was 40 degrees, and the modulus measured with the Briaud Compaction Device or BCD (Briaud et al., 2006) was 27.6 MPa.

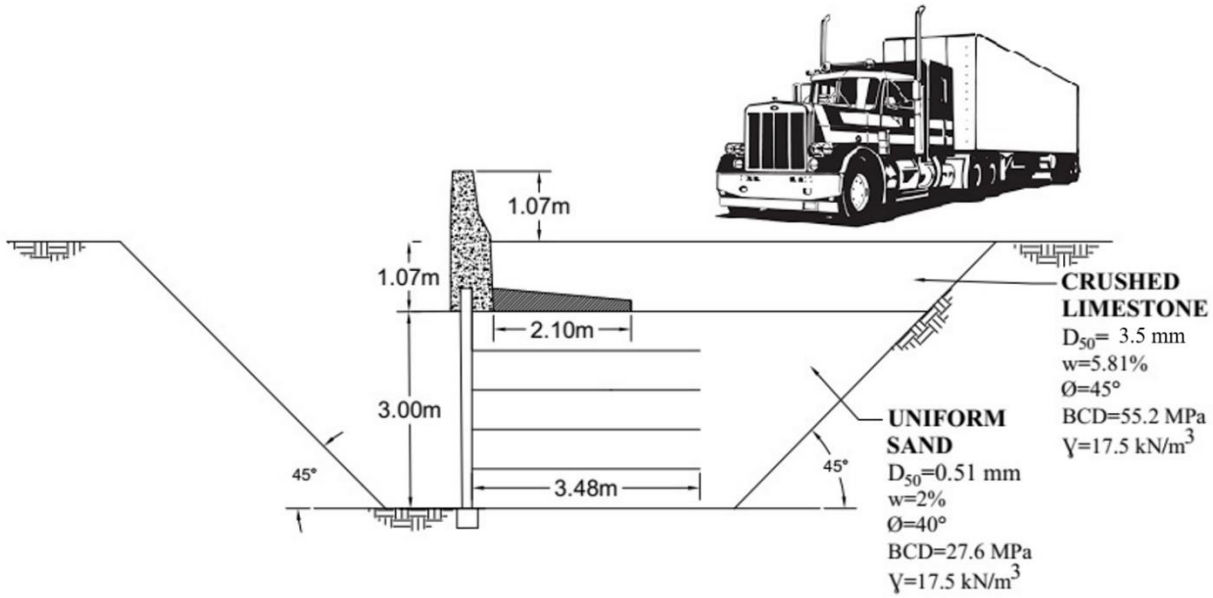


Figure 34. MSE wall / barrier / moment slab system with tractor trailer before impact.

Compacted crushed limestone was used as backfill from the bottom of the moment slab to the roadway level; the mean grain size D_{50} was 4 mm, the in-place dry unit weight was 20.5 kN/m^3, the in-place water content was 5.81%, the friction angle was 45 degrees as measured in a triaxial test, and the modulus measured with the BCD (Briaud et al., 2006) was 55.2 MPA. Fig. 34 shows a cross section of the setup before the impact. The truck was a 351.4 kN tractor trailer which hit the barrier at 80.5 km/h and at a 15-degree angle. The instruments included accelerometers placed on the frame of the tractor and on the frame of the trailer part of the truck; cameras in the x, y, and z directions; and strain gages on the MSE wall reinforcement strips. The data from the instruments were collected at 1,000 data points per second during the impact, which lasted about one second.

The test was deemed successful because the truck was properly redirected while staying upright and the barrier and wall sustained minimal damage. The maximum permanent horizontal displacement was 30 mm at the top of the barrier and 16 mm at the bottom of the barrier. The numerical simulation model was calibrated against the acceleration-time history recorded at various locations on the truck; the maximum deceleration value was 10.8 g. The calibrated numerical simulation was then used to reconstruct the impact event and gave the horizontal force on the barrier versus time history of Fig. 35, as well as a maximum dynamic displacement of 44 mm at the top of the barrier. As can be seen in Fig. 32, the first impact was the front axle of the tractor (332 kN), the second impact was the rear axle of the tractor (458.8 kN), and the third and biggest impact was the rear axle of the trailer—also called the "back slap" (744.9 kN).

A static horizontal load test was later conducted on an unused part of the barrier by pulling on the barrier horizontally and away from the wall at the height of the truck's impact; it gave a maximum static resistance of 445 kN, which corresponded to the lifting of the moment slab (Fig. 36). During the impact, the load in the reinforcement was recorded and the most highly stressed 3 m long reinforcing strip was located in the top layer of reinforcement and experienced a peak dynamic force of 9.34 kN which was reasonably well reproduced by the numerical simulation (Fig. 37). Because the calculated static capacity of a 3 m long strip in the first layer of reinforcement is 10.1 kN according to the AASHTO design rules (AASHTO, 2012), it is considered that the reinforcement was close to pull out failure during the impact. However, because the duration of the impact was so short, the associated displacement was limited and allowable; therefore, the design was acceptable. Note that the rupture load of a strip is much higher and about 58 kN. More details on this test and other tests can be found in Bligh et al. (2017).

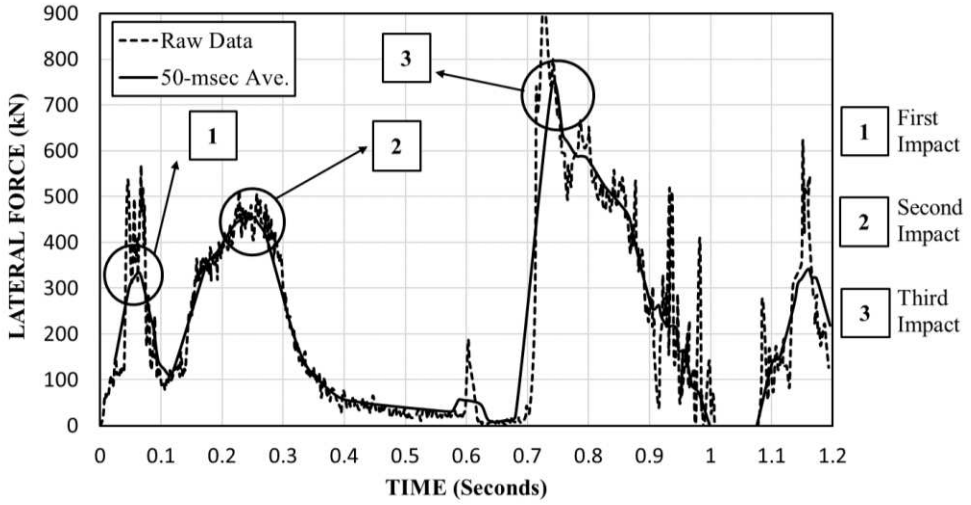


Figure 35. Impact load on the barrier during the event from numerical simulation.

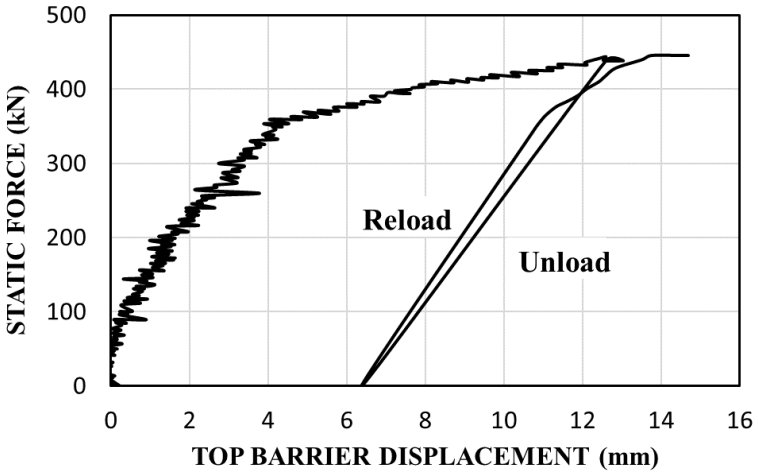


Figure 36. Static horizontal load-displacement curve for the barrier.

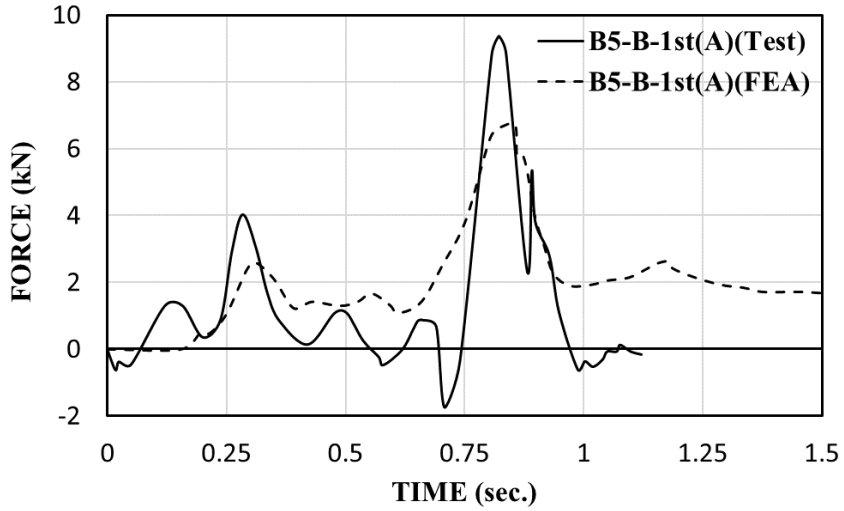


Figure 37. Tension load in the reinforcement.

If the soil is strong, a well-designed single pile may be able to stop a 66.7 kN single unit truck impacting the pile at 100 km/h within a meter or so. If the soil is soft, this is not possible; the question remained: can a group of in-line piles in a soft soil arrest such a truck? To answer this question at the National Site, a 3 m deep excavation was created and back filled with very loose uniform sand (Fig. 38). The barrier was made of 8 in-line piles connected with two beams. The sand was simply dumped in place without any compaction. It had the following properties: 16.8 kN/m^3 dry unit weight, 4.5% water content, a direct shear friction angle of 34 degrees, a SPT blow count of 1.5 bpf, pressuremeter limit pressure at 220 kPa, and pressuremeter modulus at 1900 kPa.

The piles were W14x90 steel sections (0.356 m frontal width) driven about 3 m into the loose sand with a 5.18 m spacing center to center and were connected by two steel beams HSS8x8x1/2 (200 mm x 200 mm). The truck was a 66.7 kN (mass 6,800 kg) medium duty truck that impacted the barrier head-on at 80 km/h. Before the crash test, a full-scale static load test was performed on one of the end single piles and gave an ultimate load of 60 kN for a displacement of 65 mm. The instrumentation consisted of accelerometers on the truck, strain gages on the piles, and three cameras in the x, y, and z directions. Fig. 39 shows the impact force versus time during the crash test. The impact force on the barrier was obtained by using a 3D accelerometer (mounted on the bed of the truck behind the cab) and the mass of the truck (F = ma).

Fig. 39 also shows the impact force at the point of contact obtained from the numerical simulation calculated in two ways: mass times acceleration of the bed of the truck behind the cab and directly from the finite element at the point of contact. This work was part of a larger project on barriers to protect embassies, which is documented in three PhD dissertations (Lim, 2011, Mirdamadi, 2014, Pajouh, 2015). The test was deemed successful since the truck was stopped and did not override the barrier. Numerical simulations, first calibrated against the full-scale measurements, led to design guidelines for protecting embassies against truck impact (Lim, 2011, Mirdamadi, 2014, Pajouh, 2015).

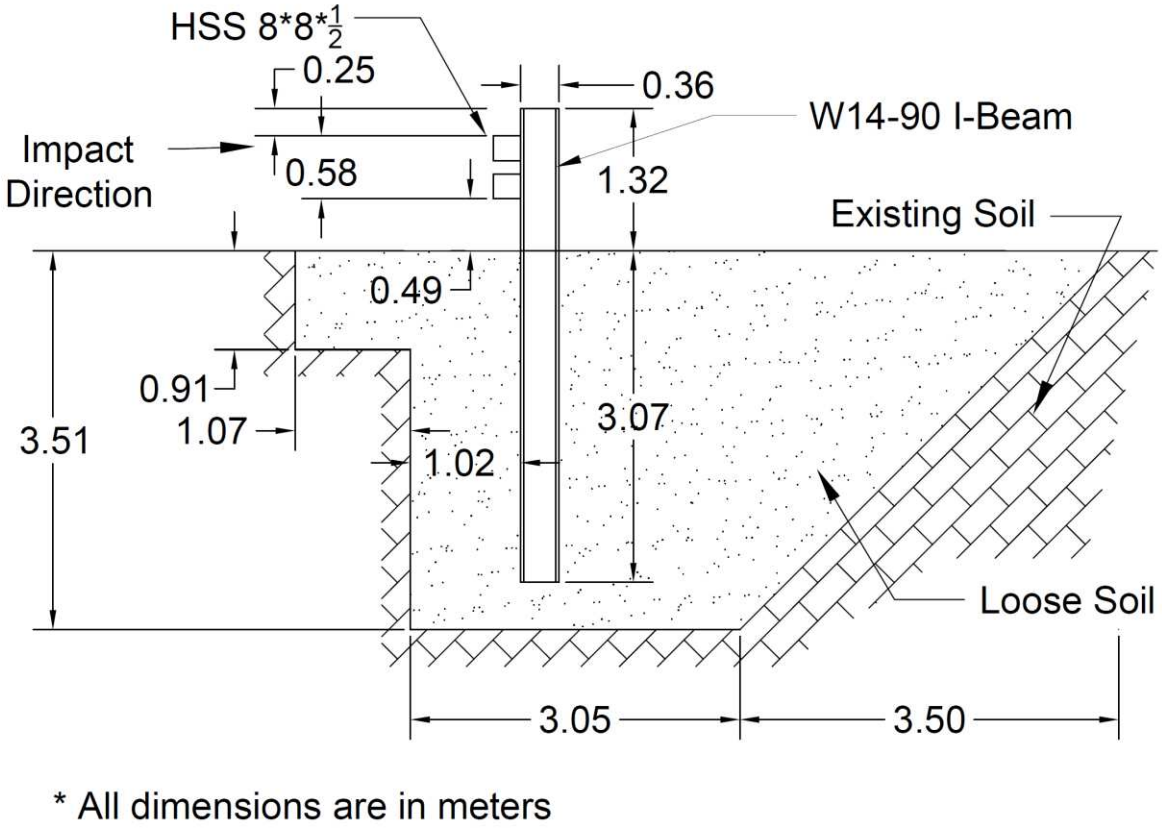


Figure 38. Barrier setup.

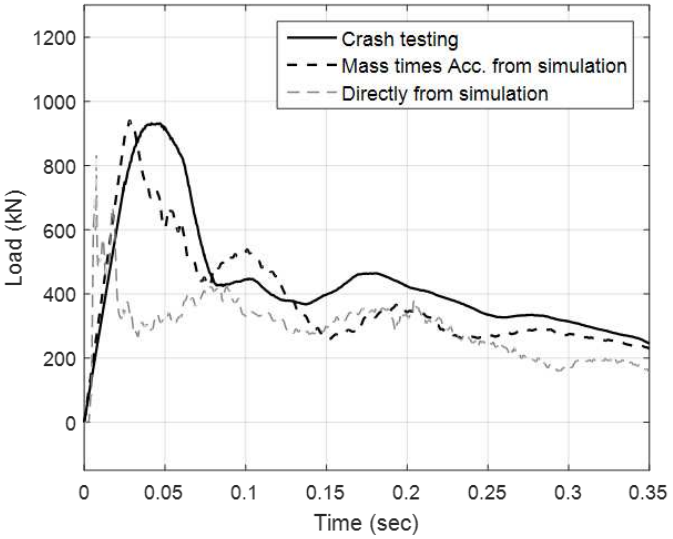


Figure 39. Impact load versus time during the crash test.

BOREHOLE EROSION TESTS

The Borehole Erosion Test (BET) is a test which was developed in 2014 (Briaud Chedid, 2015, Briaud et al., 2017) and first performed at the TAMU-NGES both clay and sand, for measuring the erodibility of the soil while drilling a borehole by the wet rotary method. The borehole is drilled to the depth of interest (e.g., 4 m). The drilling rods are removed and a mechanical borehole caliper is used to record the diameter of the hole as a function of depth; this record is called a diameter profile. The rods without the drill bit are reinserted into the borehole and water is circulated down the rods and up the annulus between the rods and the borehole wall. The water flow is recorded by a flow meter in line with the pump and the flow is maintained for a chosen time (e.g., 10 minutes). Then the rods are removed and the borehole caliper is used again to record the diameter of the hole as a function of depth. The increase in radius divided by the flow time is the erosion rate corresponding to the water velocity imparted.

By repeating this process for other velocities, the erosion function is described for all soils within the borehole depth. A typical result from a test at the site is shown in Fig. 40. The diameter profile C-0 was the zero-reading profile for the borehole as drilled, profile C-1 was obtained after 8 minutes of water flow at an average velocity of 1.07 m/s, profile C-2 after 8 minutes at an average velocity of 0.47 m/s, and profile C-3 after 9 minutes at an average velocity of 0.5 m/s. The BET has applications to bridge scour, meander migration, dam erosion, levee overtopping, and beach erosion.

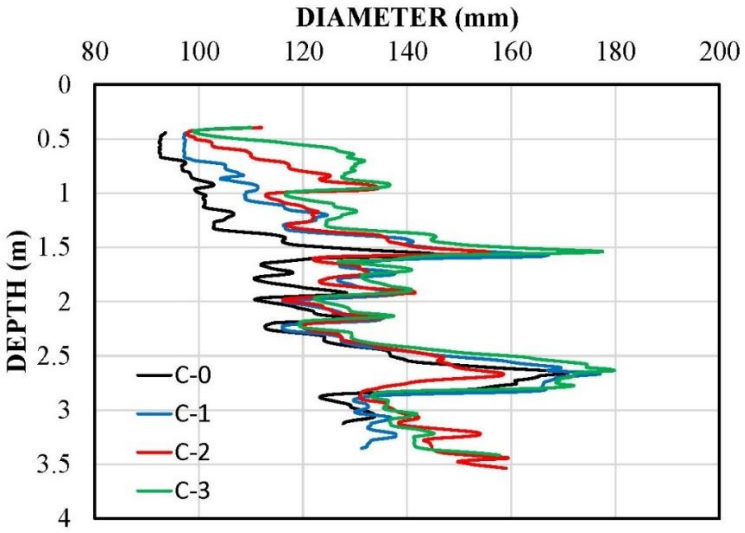


Figure 40. Borehole Erosion Test results (Briaud et al., 2015).

CONCLUSIONS

40 years of full-scale infrastructure testing at the Texas A&M University National Geotechnical Experimentation Sites have led to a wealth of data and lessons. The infrastructure testing represents a valuable resource for the geotechnical community for many years to come. Some of the conclusions reached from the projects discussed in this paper are as follows. Note that they are limited to the observations made and to the soil type tested.

1. The pressure on top of a concrete box culvert due to a 330 kN truck with tires inflated at 550 kPa and parked on top of it was negligible when the soil cover reached a depth of 1.2 m (Fig. 7). The horizontal pressure on the side of the culvert due to embankment construction and compaction were about two times the active earth pressure (Fig. 8).

2. Five large-scale spread footings loaded to 150 mm of vertical displacement showed no effect of scale, indicating the limitation of the general bearing capacity equation. The test results lead to new equations (Eq. 2) to estimate the ultimate bearing pressure, defined as the pressure leading to a settlement equal to 10% of the footing width. The load tests also show the validity of a time-dependent model to calculate the settlement at the end of the design life of the loaded footing (75 years?). A new load settlement curve method was developed to predict the load settlement for footings on sand based on the pressuremeter curve.

3. Non-Destructive Techniques (NDT) performed on the top of drilled shafts give a reasonable estimate of the length of drilled shafts but do not give a reliable estimate of defects in drilled shafts. This conclusion is based on tests conducted in 1991, and the technology has evolved significantly since; there is a need to repeat such tests to gauge how much progress has been made.

4. A poorly-constructed drilled shaft and a similar well-constructed drilled shaft were load tested to failure. The poorly-constructed drilled shaft carried only one third of the load carried by the well-constructed drilled shaft, indicating how critical quality construction is.

5. A well-instrumented 7.5 m high 50 m long top down soldier pile and lagging tieback wall was constructed and monitored for two years. The results indicated that in order to limit horizontal displacement, the wall must have sufficient vertical capacity; if not, the downdrag on the facing will force the wall to rotate around the anchor points, thus generating horizontal movement. This large anchored wall project led to a chart that can be used to choose the anchor loads given a tolerable displacement.

6. A well-instrumented 8 m high 40 m long top down soil mixing columns gravity wall was constructed and monitored for two years. The project demonstrated the soundness of the concept, provided that a soil mixing platform is constructed to bind all the columns together at the top and that the front row of columns are reinforced with an H beam within each column. The top deflection after two years was about 25 mm, as in the case of the soldier pile and lagging tieback wall.

7. Post grouting of two drilled shafts in the medium dense sand led to a 40% increase in ultimate capacity and a 60% increase in working load for 25 mm settlement.

8. A project on vibro-driven piles indicated that the piles' ultimate capacity can be approximately correlated to the rate of penetration on a site-specific basis and for a given vibro-hammer. It is estimated that these vibro-driven H piles and open-ended pipe piles carried 75% of the ultimate load that could have been carried by the same impact hammer driven piles.

9. A drilled shaft placed closely behind the face of an MSE wall can increase the load in the wall reinforcement. Based on a full-scale load test and associated numerical simulations, a pressure diagram was proposed to calculate the increase in load in the reinforcement. The maximum pressure depends on the load on the drilled shaft and on the space between the drilled shaft and the wall.

10. A full-scale crash test of a 351.4 kN tractor trailer truck impacting a barrier placed on top of an MSE wall at 80.5 km/h and at a 15-degree angle was redirected successfully while staying upright. The 3 m long MSE wall reinforcement proved to be long enough to sustain the static load of the earth pressure plus the 744.9 kN dynamic load at impact with an acceptable movement of the barrier and damage to the wall-barrier system.

11. Barriers to contain the head-on impact of a 66.7 kN truck at 80 km/h can be founded on in-line properly designed piles with embedment of the order of 3 m when the soil is loose sand. The peak dynamic force in the crash test was 950 kN.

12. The borehole erosion test is a simple in-situ test to quantify the erodibility of soil layers by giving a profile of erodibility; this is comparable with using the CPT for strength profiling.

ACKNOWLEDGEMENTS

There are many people to thank for the work that has taken place at the National Geotechnical Experimentation Site at Texas A&M University over the last 40 years. They are too numerous to be listed here but they are the sponsors of the many projects, the students who carried out the work under sometimes very difficult conditions, the colleagues who contributed a helping hand on many occasions, the visitors who brought their projects to the site, and the TAMU administration whose patience for all my requests, sometimes at the last minute, is appreciated. A special thank you goes to Mohammad Mahdavi and Anna Timchenko for redoing many of the figures in this article.

REFERENCES

American Association of State Highway and Transportation Officials, (2012). *AASHTO LRFD Bridge Design Specifications, Washington, DC*.

Ballouz, M., Nasr, G., and Briaud, J.-L. (1991). *Dynamic and Static Testing of Nine Drilled Shafts at Texas A&M University Geotechnical Research Sites*, Research Report, Dpt. of Civil Engineering, Texas A&M University.

Bligh, R.P., Briaud, J.-L., Abu-Odeh, A., Saez, D.O., Maddah, L.S., and Kim, K.M. (2017). *Design Guidelines For Test Level 3 (TL-3) Through Test Level 5 (TL-5) Roadside Barrier Systems Placed On Mechanically Stabilized Earth (MSE) Retaining Wall*, Texas A&M Transportation Institute, Final report for project NCHRP 22-20(2), Transportation Research Board, Washington D.C.

Bossher, P.J., Menclova, E., Russell, J.S., and Wahl, R.E. (1998). *Estimating Bearing Capacity of Piles Installed with Vibratory Drivers*, University of Wisconsin-Madison, Department of Civil and Environmental Engineering, US Army Corps of Engineers Technical Report CPAR-GL-98-2.

Briaud, J.-L. (1997). *National Geotechnical Experimentation Sites at Texas A&M University, Clay and Sand: A Summary*, Zachry Dpt. of Civil Engineering, Texas A&M University, College Station, USA.

Briaud, J.-L. (2007). "Spread Footings in Sand: Load Settlement Curve Approach." *Journal of Geotechnical and Geoenvironmental Engineering*, 133(8).

Briaud, J.-L. (2013). *Geotechnical Engineering: Unsaturated and Saturated Soils*, John Wiley and Sons, New York.

Briaud, J.-L. (2021). "40 Years of Full-Scale Infrastructure Testing At A National Geotechnical Experimentation Site: Clay Site." *International Journal of Geoengineering Case Histories*.

Briaud, J.-L., Ballouz, M., and Nasr, G. (2000). "Static capacity prediction by dynamic methods for three bored piles." *Journal of Geotechnical and Geoenvironmental Engineering*, 126(7).

Briaud, J.-L., Ballouz, M., and Nasr, G. (2002). "Defect and Length Prediction by NDT Methods for Nine Bored Piles." *Proc. of the International Deep Foundation Congress*, GSP 116, Orlando, Florida, Geo-Institute, ASCE.

Briaud, J.-L., and Chedid, M. (2015). *The Borehole Erosion Test – BET*, Research Report to the Texas A&M Transportation Institute Intellectual Property Committee, Zachry Dpt. of Civil Engineering, Texas A&M University.

Briaud, J.-L., Chedid, M., Chen, H.C., and Shidlovskaya, A. (2017). "The borehole Erosion Test." *Journal of Geotechnical and Geoenvironmental Engineering*, ASCE, Reston, Virginia, USA, 143(8).

Briaud, J.-L., and Gibbens, R. (1999). "Behavior of Five Spread Footings in Sand." *Journal of Geotechnical and Geoenvironmental Engineering*, 125(9), 787-797.

Briaud, J.-L., Li, Y., and Rhee, K. (2006). "BCD: A Soil Modulus Device for Compaction Control." *Journal of Geotechnical and Geoenvironmental Engineering*, ASCE, Reston, VA, 132(1).

Briaud, J.-L., Nicholson, P., and Lee, J. (2000). "Behavior of a Full-Scale VERT Wall in Sand." *Journal of Geotechnical and Geoenvironmental Engineering*, 126(9), 808-818.

Briaud, J.-L., Sanchez, M., Aghahadi, M., Bi, G., and Huang, J. (2015). *Interaction Between Drilled Shaft and Mechanically Stabilized Earth (MSE) Wall*, Texas A&M Transportation Institute, Report FHWA/TX-15/0-6715-1.

Chung, M.C., and Briaud, J.-L. (1992). *Behavior and Analysis of a Full-Scale Tieback Wall in Sand*, Research Report to FHWA, Civil Engineering, Texas A&M University.

Gardner, M.P., Jeyapalan, J.K., and James, R.W. (1986). *The Behavior of Reinforced Concrete Box Culverts Under Symmetrica1 and Unsymmetrica1 Live Loads*, Report FHWA/TX-85/ +326-2F, Texas A&M Transportation Institute, Texas A&M University System, College Station, Texas, USA.

James, R.W., Brown, D.E., Bartoskewitz, R.E., and Coyle, H.M. (1986). *Earth Pressures on Reinforced Concrete*, Report FHWA/TX-86/ 27+294-2F, Texas A&M Transportation Institute, Texas A&M University System, College Station, Texas, USA.

Kim, N.K., and Briaud, J.-L. (1992). *P y Curves for Tieback Walls*, Research Report to FHWA, Civil Engineering, Texas A&M University, August 1992.

King, P., Fernandez, A., and Pando, M. (2009). "Post Grouted Drilled Safts – A Comprehensive Case history from Texas." *Proc. of the 2009 International Foundation Congress and Equipment Exposition*, ASCE.

King, P., Fernandez, A., Pando, M.A., Briaud, J.-L., and Magbo, C.C. (2015). *Synchropile project on post grouted drilled shafts at Texas A&M University National clay and sand sites*, Zachry Dpt. of Civil Engineering, Texas A&M University, USA.

Lee, J.-H., and Briaud, J.-L. (1999). *Behavior of a Full-Scale VERT Wall in Sand*, Research Report to Geo-Con, Civil Engineering, Texas A&M University, College Station, Texas.

The open access Mission of the International Journal of Geoengineering Case Histories is made possible by the support of the following organizations:



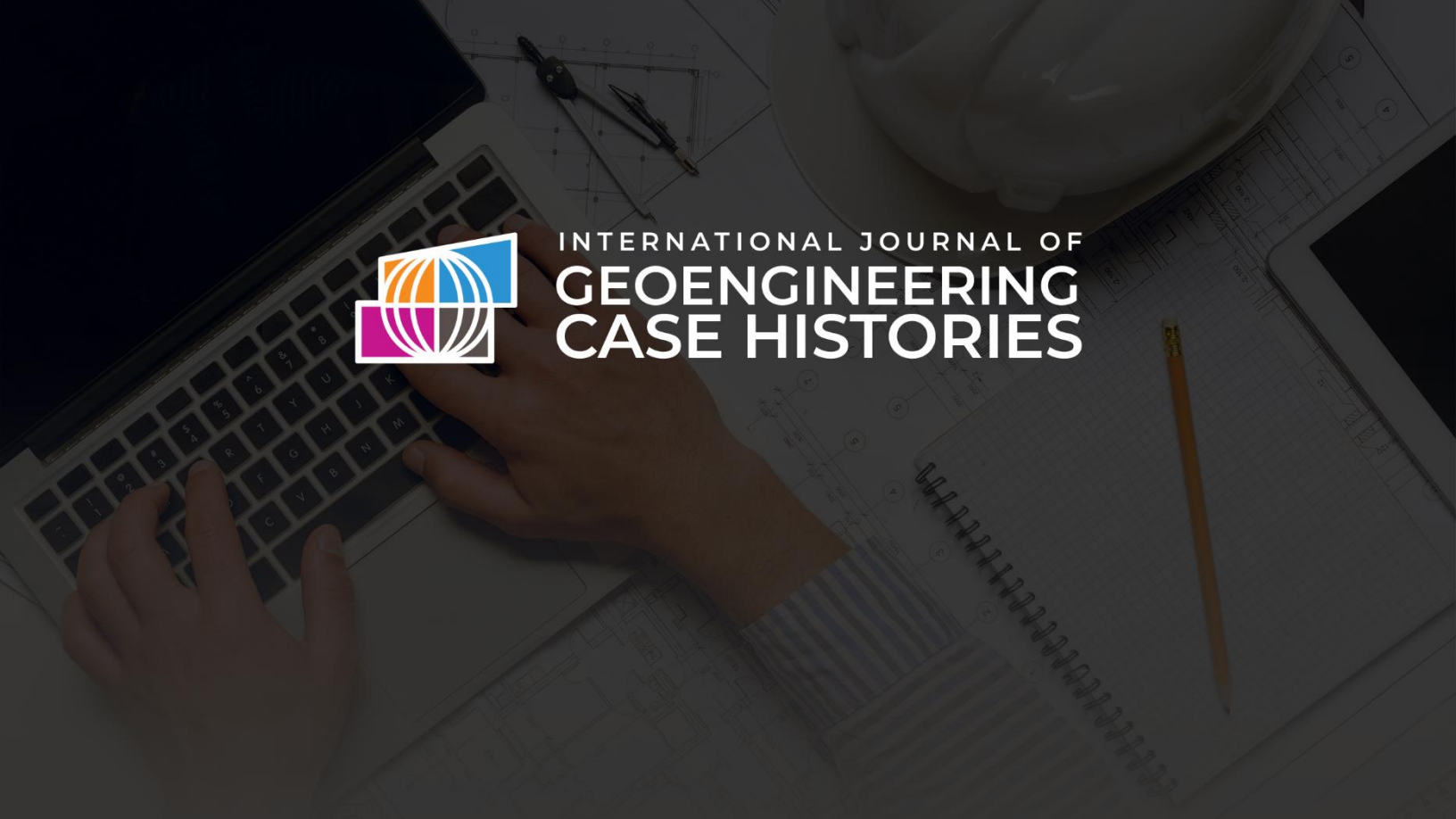








Access the content of the ISSMGE International Journal of Geoengineering Case Histories at:
https://www.geocasehistoriesjournal.org



INTERNATIONAL JOURNAL OF
GEOENGINEERING
CASE HISTORIES

The Journal's Open Access Mission is generously supported by the following Organizations:

dar
a Sidara company

Geosyntec consultants
engineers | scientists | innovators

CONETEC
MUD BAY DRILLING
LANKELMA
Geotech DRILLING

ENGEO
Expect Excellence

Access the content of the ĪSSMGE Īnternational Journal of Geoengineering Case Histories at:
www.geocasehistoriesjournal.org

Downloaded: Thursday, November 19 2026, 08:28:07 UTC